A Low-Complexity Sequential Spectrum Sensing Algorithm for Cognitive Radio

Yan Xin, *Senior Member, IEEE*, Honghai Zhang, and Lifeng Lai, *Member, IEEE*

***Abstract*—In this paper, we propose a sequential spectrum sensing algorithm for cognitive radio systems, which we term the sequential shifted chi-square test (SSCT). SSCT has the following attractive features for practical implementations. First, SSCT employs a simple test statistic and thus has a low implementation complexity. Secondly, SSCT is a sequential detection algorithm and is capable of achieving performance comparable to fixed sample size detection algorithms such as energy detection but with much reduced sensing time. Thirdly, SSCT is essentially a non-coherent detection algorithm in the sense that it does not require any deterministic knowledge of the primary signals. Lastly, SSCT is able to strike a desirable trade-off between sensing performance and sensing time particularly in the signal-to-noise ratio mismatched case. To evaluate sensing performance, we derive the exact false-alarm probability for SSCT, and develop numerical integration algorithms to compute misdetection probability and the average sample number. We further demonstrate the performance of SSCT with several numerical examples.**

***Index Terms*—Cognitive radio, energy detection, hypothesis testing, spectrum sensing, sequential detection.**

I. Introduction

As a core enabling technology for cognitive radio (CR), spectrum sensing has received considerable amount of interest recently (see [1]–[8] and recent survey papers [9], [10] and references therein). Albeit in essence a conventional signal detection problem, spectrum sensing needs to meet certain stringent requirements that stem from special characteristics of CR systems. First, it is important for the spectrum sensing algorithms to be robust to signal models as it is often difficult in practice for secondary users (SUs) to acquire complete or even partial knowledge about primary signals. Secondly, a small detection delay is essential for the spectrum sensing even under a fairly low detection signal-to-noise ratio (SNR) level with low detection error probabilities. To this end, a number of spectrum sensing algorithms including energy detection [5], generalized likelihood ratio test [11], covariance sensing [12], [13], [14] and feature detection [6] have been proposed and studied. From a practical point of view, energy detection is very attractive, primarily because it has a low implementation complexity and requires no deterministic knowledge of the signals of primary users (PUs). However, to achieve a high sensing accuracy, energy detection entails a large amount of sensing time especially when the detection SNR is low [15].

To reduce sensing time, several sequential probability ratio test (SPRT) based sensing algorithms have been proposed under various CR settings [3], [16], [17]. The main motivation of using SPRT as a sensing algorithm is that SPRT requires the shortest average sensing time for any given false-alarm and misdetection probabilities in the simple hypothesis testing case [18], [19]. However, the detection delay of SPRT is highly variable. Although the average detection delay of SPRT is less than that of the fixed sample size detection algorithm under the same error probabilities requirements, the detection delay of SPRT in a particular realization might be significantly larger than the average value. In CR systems, on the other hand, the decision must be made within a short period of sensing time [1]. In other words, sequential sensing algorithms used in practice are essentially truncated algorithms. There are two major drawbacks in the existing (truncated) SPRT-based sensing algorithms [3], [16]. First, the complexity of SPRT under practical signal models is high. In particular, the test statistic of SPRT is updated and is compared to lower- and upper-thresholds after taking each sample. Thus, the computational complexity of the test statistic determines the feasibility of SPRT. While in the simple hypothesis testing case, evaluating the test statistic of SPRT is simple, but it requires the perfect knowledge of primary signals. However, acquiring such knowledge in practice is difficult in general. In the absence of such knowledge, the evaluation of the test statistics at each time slot involves a significant amount of computation. Second, the performance of SPRT is fairly sensitive to the choices of upper- and lower-thresholds. In [18], Wald proposed an elegant method for selecting upper- and lower-thresholds for the non-truncated SPRT. Existing SPRT-based algorithms simply apply the Wald's method to select thresholds. Such selection does not work well for truncated sensing algorithms since it leads to an increase in detection error probabilities.

The goals of this paper are twofold: 1) to design low complexity sensing algorithms that have good performance and are amenable to implementation; and 2) to develop the corresponding performance evaluation techniques that can guide the proper choice of design parameters (as opposed to the existing ad hoc approach). To this end, we develop a truncated sequential spectrum sensing algorithm, called the sequential shifted chi-square test (SSCT). SSCT possesses several attractive features: 1) similar to energy detection, SSCT

Manuscript received October 29, 2012; revised April 14, 2013 and June 26, 2013. The work of L. Lai was supported by the National Science Foundation under grant DMS-12-65663. This paper was presented in part at the IEEE Global Telecommunications Conference (GLOBECOM), Honolulu, Hawaii, USA, November 2009.

Y. Xin is with Samsung Research America Dallas (SRA-D), 1301 E Lookout Drive, Richardson, TX, 75082 USA (e-mail: yan.xin@samsung.com).

H. Zhang is with Google Inc., 822 NW 64th St., Seattle, WA, 98107 USA (e-mail: honghaiz@google.com).

L. Lai is with the Department of Electrical and Computer Engineering, Worcester Polytechnic Institute, Worcester, MA, 01609, USA (e-mail: llai@wpi.edu).

Digital Object Identifier 10.1109/JSAC.2014.140302

requires only the knowledge on the noise power and does not require any deterministic knowledge of primary signals; 2) compared to fixed-sample-size detection algorithms such as energy detection, SSCT is capable of achieving a comparable detection performance with much reduced average sensing time; 3) in comparison with existing SPRT-based sensing algorithms [16], SSCT has a much simpler test statistic and has a lower implementation complexity; and 4) SSCT offers desirable flexibility to strike a trade-off between detection performance and sensing delay when the operating SNR is higher than the minimum detection SNR. Furthermore, to evaluate the detection performance of SSCT and hence guide the proper choice of parameters, which is typically a challenging task, we derive the exact false-alarm probability and provide numerical integration algorithms to compute the misdetection probability and the average sample number (ASN) in a recursive manner.

Furthermore, we notice that the problem of evaluating the false-alarm probability of SSCT is similar to the exact operating characteristic (OC) evaluation problem associated with truncated sequential life tests (T-SLT) with the exponential distribution [20], [21]. The latter problem has been solved by Woodall and Kurkjian [20]. Despite the similarity of these two problems, the Woodall-Kurkjian approach cannot be directly applied to evaluate the false-alarm probability of SSCT. In addition, the Woodall-Kurkjian approach is not applicable to evaluate ASN of T-SLT involving exponential distribution [21]. As a byproduct, our approach for evaluating the false-alarm probability of SSCT can be readily modified to evaluate ASN for T-SLT in the exponential case.

The remainder of this paper is organized as follows. Section II presents the problem formulation and provides necessary preliminaries on the energy detection based and SPRT-based sensing algorithms. Section III introduces SSCT and its equivalent test procedure. Section IV deals with the evaluation of the error probabilities of SSCT. In particular, this section provides an exact result for the false-alarm probability, and a numerical integration algorithm to recursively compute the misdetection probability. Section V presents an evaluation result on ASN of SSCT, while Section VI provides several numerical examples. Finally, Section VII concludes the paper.

Notation: Boldface upper and lower case letters are used to denote matrices and vectors, respectively; $\boldsymbol{I}_k$ denotes a $k \times k$ identity matrix; $E[\cdot]$ denotes the expectation operator. $(\cdot)^T$ denotes the transpose operation; $\mathbf{1}_k$ denotes a $k \times 1$ vector whose entries are all ones; $\aleph_p^q$ denotes a set of consecutive integers from p to q, i.e., $\aleph_p^q := \{p, \ldots, q\}$, where p is a non-negative integer and q is a positive integer greater than p or $+\infty$; $(\cdot)^c$ denotes a complement of a set; $\mathbb{I}_{\{x \geq t\}}$ denotes an indicator function defined as $\mathbb{I}_{\{x \geq t\}} = 1$ if $x \geq t$ and $\mathbb{I}_{\{x \geq t\}} = 0$ if $x < t$, where x is a variable and t is a constant.

II. Problem Formulation and Preliminaries

In this section, we start by presenting a statistical formulation of the spectrum sensing problem for a single SU CR system. We next give a brief overview on two sensing algorithms that are closely related to SSCT: energy detection and a SPRT-based sensing algorithm.

A. Problem Formulation

In this paper, we assume that there is a single SU in the CR system, which is allowed to access the licensed spectrum of PU in an opportunistic manner. Upon receiving the signal samples denoted by r_i, SU is required to detect whether there are primary signals or not before using the licensed spectrum. We use $s_i,\ i = 1, 2, \ldots$ to denote the primary signal samples. Such a signal detection problem can be written as the following classic binary hypothesis testing problem:

$$\begin{cases} H_0 : r_i = w_i,\ i = 1, 2, \ldots, \\ H_1 : r_i = h s_i + w_i,\ i = 1, 2, \ldots, \end{cases} \tag{1}$$

where w_i denotes additive white Gaussian noise (AWGN) with zero mean and variance $\sigma_w^2/2$ per dimension, i.e., $w_i \sim \mathcal{CN}(0, \sigma_w^2)$, and h is the channel coefficient between PU and SU. We further assume that the channel coefficient h is a constant during the sensing process, and the primary signal samples s_i are independent and identically distributed (i.i.d.).

B. Preliminaries

1) Energy Detection: Energy detection is a fixed sample size sensing algorithm in the sense that the decision is made after collecting a fixed number of samples, say M. Let $\boldsymbol{r}$ be the $1 \times M$ received signal vector defined as $\boldsymbol{r} := [r_1, r_2, \ldots, r_M]$. In energy detection, we compute the energy of $\boldsymbol{r}$ and compare it with a predetermined value. Mathematically, the testing procedure is described as: Accept H_1, if $T(\boldsymbol{r}) := \sum_{i=1}^{M} |r_i|^2 \geq \gamma_{\text{ed}}$; Accept H_0, if $T(\boldsymbol{r}) < \gamma_{\text{ed}}$, where γ_{ed} denotes a threshold for energy detection.

Since w_i is a zero mean complex Gaussian random variable (RV) with variance $\sigma_w^2/2$ per dimension, $2T(\boldsymbol{r})/\sigma_w^2$ is a central chi-square RV with $2M$ degrees of freedom under H_0, and is a noncentral chi-square RV with $2M$ degrees of freedom and non-centrality parameter $2|h|^2 \sum_{i=1}^{M} |s_i|^2/\sigma_w^2$ under H_1 conditioning on $|s_i|^2\ , i = 1, \ldots, M$. As M increases, $2|h|^2 \sum_{i=1}^{M} |s_i|^2/\sigma_w^2$ approaches $2M|h|^2\sigma_s^2/\sigma_w^2$, where σ_s^2 denotes the average symbol energy. Define $\texttt{SNR}_m$ as the minimum detection SNR, at which the requirements on the target false-alarm and misdetection probabilities are satisfied. The minimum detection SNR is a design parameter, which depends on implementation scenarios but is not directly related to a particular channel realization. In practice, it is highly likely that $\texttt{SNR}_m$ is different from the exact operating SNR, which is defined as $|h|^2\sigma_s^2/\sigma_w^2$. The exact operating SNR depends on the channel gain h between PU and SU, which is difficult to acquire in practice. To distinguish these two different SNRs, we denote by $\texttt{SNR}_o$ the exact operating SNR.

It follows directly from the central limit theorem (CLT) that as M approaches infinity, the distribution of $2T(\boldsymbol{r})/\sigma_w^2$ converges to a normal distribution as follows [2]: $2T(\boldsymbol{r})/\sigma_w^2 \sim \mathcal{N}(2M, 4M)$ under H_0 while $2T(\boldsymbol{r})/\sigma_w^2 \sim \mathcal{N}\big(2M(1 + \texttt{SNR}_m), 4M(1 + 2\texttt{SNR}_m)\big)$ under H_1. Let $\bar{\alpha}_{\text{ed}}$ and $\bar{\beta}_{\text{ed}}$ be the target false-alarm and misdetection probabilities, respectively. Generally speaking, the number of required signal samples M is determined by $\bar{\alpha}_{\text{ed}}$ and $\bar{\beta}_{\text{ed}}$. We use $M_{\text{ed}}^{\min}$ to denote the minimum number of sensing samples required to meet the target $\bar{\alpha}_{\text{ed}}$ and $\bar{\beta}_{\text{ed}}$ requirements when the detection SNR is

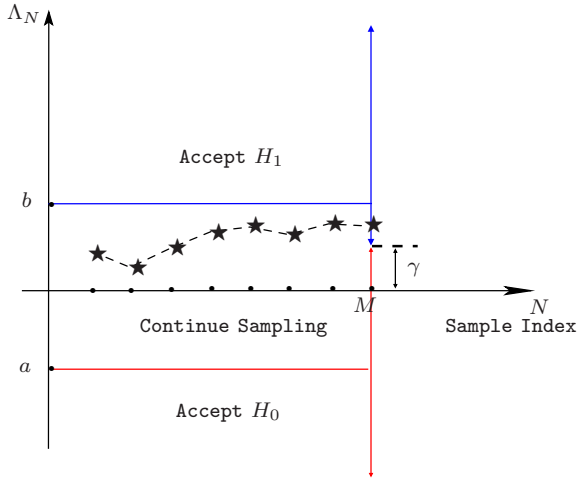

Fig. 1. The test region of SSCT.

$\mathtt{SNR}_m$. As shown in [1], we have

$$M_{\text{ed}}^{\min} = \left\lceil \mathtt{SNR}_m^{-2}\left[\mu - \nu \cdot \sqrt{2\mathtt{SNR}_m + 1}\right]^2 \right\rceil \tag{2}$$

where $\mu := Q^{-1}(\bar{\alpha}_{\text{ed}})$, $\nu := Q^{-1}(1-\bar{\beta}_{\text{ed}})$, and $\lceil x \rceil$ denotes the smallest integer greater than or equal to x, $\mathcal{Q}(\cdot)$ denotes the complementary cumulative distribution function of the standard normal RV, i.e., $\mathcal{Q}(x) := (2\pi)^{-1/2}\int_x^\infty e^{-t^2/2}dt$, and $\mathcal{Q}^{-1}(\cdot)$ denotes its inverse function. It is evident from (2) that for energy detection, the minimum number of samples is proportional to $\mathtt{SNR}_m^{-2}$ for a sufficiently small $\mathtt{SNR}_m$ [15].

It is clear from the description above that energy detection has a simple test statistic and a low implementation complexity [5]. In addition, known as a form of non-coherent detection, energy detection requires only the knowledge of noise power and does not rely on any deterministic knowledge about the primary signal s_i. However, one major drawback of the energy detection is that, at a low SNR, it requires a large amount of sensing time to achieve low detection error probabilities.

2) A SPRT-Based Sensing Algorithm: In comparison with a fixed-sample-size detection such as energy detection, SPRT can achieve the same detection performance with a much reduced ASN [19]. We next investigate a SPRT based sensing algorithm that relies on the amplitude squares of the received signal samples [3], [16].

To simplify the description, we review a case in which the amplitude squares of primary signals, $|s_i|^2,\ i = 1, 2, \ldots$, are perfectly known at SU. In this case, the spectrum sensing problem formulated in (1) becomes a simple hypothesis testing problem, which is the original setup considered by Wald [18]. Normalize $|r_i|^2$ as $v_i := 2|r_i|^2/\sigma_w^2$ for the convenience of derivation. Note that under H_0, v_i is an exponential RV with rate parameter $1/2$, and under H_1, v_i is a noncentral chi-square RV (conditional on $|s_i|^2$) with two degrees of freedom and non-centrality parameter λ_i that can be readily obtained as $\lambda_i = 2|h|^2|s_i|^2/\sigma_w^2$. Hence, the probability density function (PDF) of v_i under H_0 is

$$p_{H_0}(v_i) = \frac{1}{2}e^{-v_i/2} \tag{3}$$

whereas under H_1, the PDF of v_i (conditional on λ_i) is

$$p_{H_1}(v_i|\lambda_i) = \frac{1}{2}e^{-(v_i+\lambda_i)/2} I_0(\sqrt{\lambda_i v_i}) \tag{4}$$

where $I_0(\cdot)$ is the zeroth-order modified Bessel function of the first kind. After collecting N samples, we can express the accumulative log-likelihood ratio as

$$\begin{aligned} L_N(\boldsymbol{v}_N|\boldsymbol{\lambda}_N) &= \log\frac{p_{\boldsymbol{v}|H_1}(\boldsymbol{v}_N|\boldsymbol{\lambda}_N)}{p_{\boldsymbol{v}|H_0}(\boldsymbol{v}_N)} = \sum_{i=1}^{N} z_i \\ &= -\sum_{i=1}^{N}\lambda_i/2 + \sum_{i=1}^{N}\log I_0(\sqrt{\lambda_i v_i}) \end{aligned} \tag{5}$$

where $\boldsymbol{v}_N := (v_1, v_2, \ldots, v_N)$, $z_i := \log\left(p_{H_1}(v_i|\lambda_i)/p_{H_0}(v_i)\right)$, and $\boldsymbol{\lambda}_N := (\lambda_1, \lambda_2, \ldots, \lambda_N)$. The test procedure is given as follows: Accept H_1, if $L_N(\boldsymbol{v}_N|\boldsymbol{\lambda}_N) \geq b_L$; Accept H_0, if $L_N(\boldsymbol{v}_N|\boldsymbol{\lambda}_N) \leq a_L$; and continue sensing, if $a_L < L_N(\boldsymbol{v}_N|\boldsymbol{\lambda}_N) < b_L$. In [18], Wald specified a particular choice of thresholds a_L and b_L for the *non-truncated* SPRT as follows: $a_L = \log\bar{\beta}_{\text{sprt}}/(1-\bar{\alpha}_{\text{sprt}})$, and $b_L = \log(1-\bar{\beta}_{\text{sprt}})/\bar{\alpha}_{\text{sprt}}$ where $\bar{\alpha}_{\text{sprt}}$ and $\bar{\beta}_{\text{sprt}}$ denote the target false-alarm and misdetection probabilities, respectively. For a non-truncated SPRT, the Wald's choice on a_L and b_L yields true false-alarm and misdetection probabilities that are fairly close to the target ones.

Let z be a RV having the same PDF as z_i. It has been pointed out in [22] that, in SPRT, if hypotheses H_0 and H_1 are distinct, then $E_{H_0}(z) < 0 < E_{H_1}(z)$, where $E_{H_i}(\cdot)$ denotes the expectation under $H_i,\ i = 1, 2$. As evident from (5), one shortcoming of this SPRT-based sensing algorithm is that the test statistic contains a modified Bessel function, which may result in a high implementation complexity. When the perfect knowledge of the instantaneous amplitude squares of the primary signals is not available, PDF under H_1 is not completely known, i.e., the alternative hypothesis is composite. Generally speaking, two approaches, the Bayesian approach and the generalized likelihood ratio test, can be used to deal with such a case. In the Bayesian approach, *a prior* PDF of the amplitude squares of the primary signals is required and multiple summations over all possible amplitudes of the primary signals need to be performed, whereas in the generalized likelihood ratio test, a maximum likelihood estimation (MLE) of the amplitude squares of the primary signals is needed [11]. Either of these two approaches, however, leads to a considerable increase in the implementation complexity.

III. A Low-Complexity Sequential Spectrum Sensing Algorithm

We now propose a low-complexity sequential spectrum sensing algorithm depicted as follows:

$$\Lambda_N = \sum_{i=1}^{N}\left(|r_i|^2 - \Delta\right), \tag{6}$$

in which Δ is a fixed and predetermined parameter. Suppose that the detector has a decision deadline M. That is, the

detector needs to make a decision within M samples. We propose the following test procedure

$$\texttt{Accept } H_1: \quad \text{if } \Lambda_N \geq b \text{ for } 0 < N \leq M-1, \text{ or if } \Lambda_M \geq \gamma; \tag{7}$$

$$\texttt{Accept } H_0: \quad \text{if } \Lambda_N \leq a \text{ for } 0 < N \leq M-1, \text{ or if } \Lambda_M < \gamma; \tag{8}$$

$$\texttt{Continue Sensing}: \quad \text{if } \Lambda_N \in (a,b) \text{ for } 0 < N \leq M-1 \tag{9}$$

where a, b, and γ denote three predetermined and fixed constants satisfying the following conditions: $a < 0$, $b > 0$, and $\gamma \in (a,b)$. In statistical term, the test procedure given in (7)–(9) is nothing but a *truncated* sequential test. As depicted in Fig. 1, the stopping boundaries of the test region consist of horizonal lines b and a, which we call the upper- and lower-boundary respectively. Notice that each term $|r_i|^2 - \Delta$ in Λ_N is nothing but a shifted chi-square RV. Hence, we simply name this sensing algorithm described in (7)-(9) *sequential shifted chi-square test* (SSCT). As can be seen from (6), SSCT has a simple test statistic that contains only the amplitude squares of the received signals and the parameter Δ.

Let r be a RV with the same PDF as $|r_i|^2 - \Delta$, which is the ith incremental term in the test statistic (6). Similar to the SPRT case, we choose $\sigma_w^2 < \Delta < \sigma_w^2(1+\texttt{SNR}_m)$ to ensure $E_{H_0}(r) < 0 < E_{H_1}(r)$. In SSCT, we have $E_{H_0}(r) = \sigma_w^2 - \Delta$ and $E_{H_1}(r) = \sigma_w^2(1+\texttt{SNR}_o) - \Delta$. Using $\texttt{SNR}_m \leq \texttt{SNR}_o$ and $\sigma_w^2 < \Delta < \sigma_w^2(1+\texttt{SNR}_m)$, we always have $E_{H_0}(r) < 0 \leq \texttt{SNR}_o - \texttt{SNR}_m < E_{H_1}(r)$. Note that with this choice, the constant Δ depends on the minimum detection SNR instead of the exact operating SNR. Normalize the test statistic Λ_N by $\sigma_w^2/2$ and define $\bar{\Lambda}_N := 2\Lambda_N/\sigma_w^2$. We rewrite (6) as

$$\bar{\Lambda}_N = \sum_{i=1}^{N} (v_i - 2\Delta/\sigma_w^2) \tag{10}$$

where $v_i := 2|r_i|^2/\sigma_w^2$. Let ξ_N denote the sum of v_i for $i = 1, \ldots, N$, i.e., $\xi_N = \sum_{i=1}^{N} v_i$ and let $\bar{\Delta}$ denote $2\Delta/\sigma_w^2$. Applying this notation, we rewrite $\bar{\Lambda}_N$ as $\bar{\Lambda}_N = \xi_N - N\bar{\Delta}$. We let $\bar{\Lambda}_0$ and ξ_0 be 0 for notational simplicity. We further define a_i and b_i as: $a_i = 0$ for $\aleph_0^P$, $a_i = \bar{a} + i\bar{\Delta}$ for $i \in \aleph_{P+1}^{\infty}$, and $b_i = \bar{b} + i\bar{\Delta}$ for $b \in \aleph_0^{\infty}$, where $\bar{a} := 2a/\sigma_w^2$, $\bar{b} := 2b/\sigma_w^2$, and P denotes the largest integer not greater than $-a/\Delta$, i.e., $P := \texttt{floor}(-a/\Delta)$. Applying the notation $\xi_N = \sum_{i=1}^{N} v_i$, we express the test procedure (7)–(9) as

$$\texttt{Accept } H_1: \quad \texttt{if } \xi_N \geq b_N \text{ for } 0 < N \leq M-1, \texttt{ or if } \xi_M \geq \bar{\gamma}_M; \tag{11}$$

$$\texttt{Accept } H_0: \quad \texttt{if } \xi_N \leq a_N \text{ for } 0 < N \leq M-1, \texttt{ or if } \xi_M < \bar{\gamma}_M; \tag{12}$$

$$\texttt{Continue Sensing}: \quad \texttt{if } \xi_N \in (a_N, b_N) \text{ for } 0 < N \leq M-1 \tag{13}$$

where $\bar{\gamma}_M = \bar{\gamma} + M\bar{\Delta}$ with $\bar{\gamma} := 2\gamma/\sigma_w^2$. The corresponding test region is depicted in Fig. 2, where the stopping boundaries comprise two slant line segments. Define α_{ssct} and β_{ssct} as the false-alarm and misdetection probabilities of SSCT, respectively.

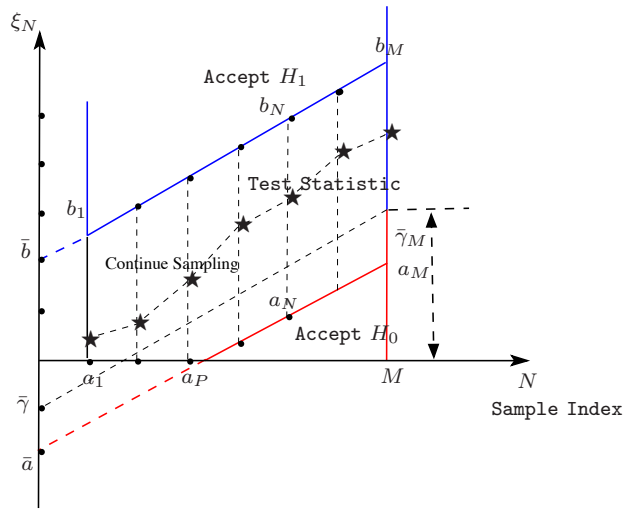

Fig. 2. The test region of the transformed test procedure.

The issue of how to select thresholds a, b, and γ is critical to the performance of SSCT. In [18], Wald proposed a method to select appropriate thresholds for the non-truncated SPRT. Since the proposed test procedure in (7)-(9) is a truncated sequential test and is not necessarily a SPRT, the thresholds selected by the Wald's method cannot meet target detection performance requirements in general.

As a result, an alternative approach to select thresholds is needed. Typically, the thresholds a, b, γ, the parameter Δ, and the truncated size M are selected *beforehand and off-line*, either purposefully or randomly, and the corresponding α_{ssct} and β_{ssct} are then computed. If the resulted α_{ssct} and β_{ssct} do not meet the requirement, the thresholds and truncated size are subsequently adjusted. This process continues until a desirable error probability performance is obtained. In the above process, the key and challenging step is to accurately and efficiently evaluate α_{ssct} and β_{ssct} as well as ASN for any prescribed thresholds a, b, γ, the parameter Δ, and the truncated size M. In the following section, we will show how to evaluate these quantities for SSCT.

IV. Evaluations of False-Alarm and Misdetection Probabilities

In this section, we present the exact false-alarm probability result, and a numerical integration algorithm that obtains the misdetection probability in a recursive manner [23] for any given thresholds. We start by introducing some preparatory tools, including three integrals that will be used for evaluating the false-alarm probability.

A. Preparatory Tools

We introduce the first integral as follows:

$$f_{\boldsymbol{\chi}_k}^{(k)}(\xi) = \int_{\chi_k}^{\xi} d\xi_k \int_{\chi_{k-1}}^{\xi_k} d\xi_{k-1} \cdots \int_{\chi_1}^{\xi_2} d\xi_1, \ k \geq 1 \tag{14}$$

and $f_{\boldsymbol{\chi}_k}^{(k)}(\xi) = 1$ for $k = 0$, where $\boldsymbol{\chi}_0 = \emptyset$ and $\boldsymbol{\chi}_k := [\chi_1, \ldots, \chi_{k-1}, \chi_k]$ with $0 \leq \chi_1 \leq \ldots \leq \chi_k$. The superscript k and the subscript $\boldsymbol{\chi}_k$ are used to indicate that $f_{\boldsymbol{\chi}_k}^{(k)}(\xi)$ is

a k-fold multiple integral with ordered lower limits specified by $\boldsymbol{\chi}_k$. Evidently, the integral $f^{(k)}_{\boldsymbol{\chi}_k}(\xi)$ is a polynomial in ξ of degree k. Lemma 1 shows that the exact value of $f^{(k)}_{\boldsymbol{\chi}_k}(\xi)$ can be computed recursively (refer to Appendix A for the proof).

Lemma 1: The integral $f^{(k)}_{\boldsymbol{\chi}_k}(\xi)$ is given by

$$f^{(k)}_{\boldsymbol{\chi}_k}(\xi)=\sum_{i=0}^{k-1}\frac{f_i^{(k)}(\xi-\chi_{i+1})^{k-i}}{(k-i)!}+f_k^{(k)} \tag{15}$$

where $f_i^{(k)},\ i=0,\ldots,k$, for $k\geq 1$ can be obtained recursively as follows: $f_i^{(k)}=f_i^{(k-1)},\ i\in\aleph_0^{k-1}$ and

$$f_k^{(k)}=-\sum_{i=0}^{k-1}\frac{f_i^{(k-1)}}{(k-i)!}(\chi_k-\chi_{i+1})^{k-i} \tag{16}$$

with $f_0^{(0)}=1$. For the case where $\chi_1=\chi_2=\ldots=\chi_k=\chi$, the coefficients $f^{(k)}_{\boldsymbol{\chi}_k}$ is given by

$$f^{(k)}_{\boldsymbol{\chi}_k}=\frac{1}{k!}(\xi-\chi)^k. \tag{17}$$

Additionally, the integral $f^{(k)}_{\boldsymbol{\chi}_k}(\xi)$ has the following useful properties: 1) *Differential Property:* $df^{(k)}_{\boldsymbol{\chi}_k}(\xi)/d\xi=f^{(k-1)}_{\boldsymbol{\chi}_{k-1}}(\xi)$ with $\boldsymbol{\chi}_{k-1}=[\chi_1,\ldots,\chi_{k-1}]$ and $k\geq 2$; 2) *Scaling Property:* $f^{(k)}_{t\boldsymbol{\chi}_k}(t\xi)=t^k f^{(k)}_{\boldsymbol{\chi}_k}(\xi)$ for $t>0$; 3) *Shift Property:* $f^{(k)}_{\boldsymbol{\chi}_k-\delta\mathbf{1}_k}(\xi-\delta)=f^{(k)}_{\boldsymbol{\chi}_k}(\xi)$.

It is noteworthy to mention that the formula (15) together with scaling and shift properties are particularly useful in reducing round-off errors when evaluating $f^{(k)}_{\boldsymbol{\chi}_k}(\xi)$. These two properties will be used to ensure the numerical stability of the false-alarm probability computation method presented later in this section. The second integral that will be useful is

$$I^{(0)}:=1,\ \text{and}\ I^{(n)}:=\int_{\Omega^{(n)}}\cdots\int d\boldsymbol{\xi}_n,\ n\geq 1 \tag{18}$$

where $\boldsymbol{\xi}_n:=[\xi_1,\xi_2,\ldots,\xi_n]$ with $0\leq\xi_1\leq\xi_2\cdots\leq\xi_n$, and $\Omega^{(n)}=\{(\xi_1,\xi_2,\ldots,\xi_n):0\leq\xi_1\leq\cdots\leq\xi_n;a_i<\xi_i<b_i,i\in\aleph_1^n\}$. For $n=1$, we have $I^{(1)}=\int_{a_1}^{b_1}d\xi_1=b_1-a_1$. We define c and d as two parameters satisfying $0\leq c<d$, $a_{N-1}\leq c\leq b_N$ and $a_N\leq d$. For $N\geq 2$, we define the following vector

$$\boldsymbol{\psi}^N_{n,c}=\begin{cases}[\underbrace{b_{n+1},\ldots,b_{n+1}}_{Q},\underbrace{a_{Q+n+1},\ldots,a_{N-1},c}_{N-Q-n}], n\in\aleph_0^{N-Q-2}\\ [\underbrace{b_{n+1},\ldots,b_{n+1},c}_{N-n}], n\in\aleph_{N-Q-1}^{s-1}\\ b_{n+1}\mathbf{1}_{N-n}, n\in\aleph_s^{N-2}\end{cases}$$

where s and Q denote the integers satisfying $b_s<c\leq b_{s+1}$ and $a_Q\leq b_1<a_{Q+1}$ respectively. Let us define $\boldsymbol{A}_i$ as an $(N-n)\times(N-n-i)$ matrix $\boldsymbol{A}_i=[\boldsymbol{I}_{N-i-n}|\mathbf{0}_{(N-i-n)\times i}]^T$ with $i\in\aleph_1^{N-n}$. In addition, we define the following vectors $\boldsymbol{\psi}^{N-i}_{n,c}=\boldsymbol{\psi}^N_{n,c}\cdot\boldsymbol{A}_i,\ i\in\aleph_1^{N-n}\boldsymbol{a}^{n_2}_{n_1}=[a_{n_1+1},\ldots,a_{n_2}],\ n_2\geq n_1\geq 0$, where $\boldsymbol{\psi}^{N-i}_{n,c}$ is an $(N-i-n)\times 1$ vector and $\boldsymbol{a}^{n_2}_{n_1}$ is an $(n_1-n_2)\times 1$ vector. If $n_1=n_2$, we define $a^{n_2}_{n_1}$ as $\emptyset$. In what follows, we show that we can compute the exact value of $I^{(N)}$ in (18) recursively (refer to Appendix B for the proof).

Lemma 2: The exact value of the integral $I^{(N)}$ is given by

$$I^{(N)}=f^{(N)}_{\boldsymbol{a}_0^N}(b_N)-\begin{cases}\mathbb{I}_{\{N\geq 2\}}\displaystyle\sum_{n=0}^{N-2}\frac{(b_N-b_{n+1})^{N-n}I^{(n)}}{(N-n)!}, & N\in\aleph_1^Q\\ \displaystyle\sum_{n=0}^{N-2}f^{(N-n)}_{\boldsymbol{\psi}^N_{n,a_N}}(b_N)I^{(n)}, & N\in\aleph_{Q+1}^{\infty}\end{cases} \tag{19}$$

with $I^{(0)}=1$.

The third integral is given by

$$J^{(N)}_{c,d}(\theta):=\int_{\Upsilon^{(N)}_{c,d}}\cdots\int e^{-\theta\xi_N}d\boldsymbol{\xi}_N \tag{20}$$

where $\theta>0$, $N\geq 1$, and $\Upsilon^{(N)}_{c,d}:=\{(\xi_1,\ldots,\xi_N):0\leq\xi_1\leq\ldots\leq\xi_N;a_i<\xi_i<b_i,i\in\aleph_1^{N-1};c<\xi_N<d\}$. Recall that c and d are two non-negative numbers satisfying $a_{N-1}\leq c\leq b_N$ and $0\leq c<d$ and $d\geq a_N$. We define the following function

$$g^{(n)}_{c,d}(\theta)=\begin{cases}I^{(n)}\Big[\theta^{n-N}e^{-\theta b_{n+1}}-\displaystyle\sum_{i=1}^{N-n}\theta^{-i}\times\\ \qquad f^{(N-n-i)}_{b_{n+1}\mathbf{1}_{N-n-i}}(d)e^{-\theta d}\Big],\ c\leq b_1,n\in\aleph_0^{N-2}\\ I^{(n)}\displaystyle\sum_{i=1}^{N-n}\theta^{-i}\Big[f^{(N-n-i)}_{\boldsymbol{\psi}^{N-i}_{n,c}}(c)e^{-\theta c}-\\ \qquad f^{(N-n-i)}_{\boldsymbol{\psi}^{N-i}_{n,c}}(d)e^{-\theta d}\Big],\ c>b_1,n\in\aleph_0^{s-1}\\ I^{(n)}\Big[\theta^{n-N}e^{-\theta b_{n+1}}-\displaystyle\sum_{i=1}^{N-n}\theta^{-i}\times\\ \qquad f^{(N-n-i)}_{b_{n+1}\mathbf{1}_{N-n-i}}(d)e^{-\theta d}\Big],\ c>b_1,n\in\aleph_s^{N-2}.\end{cases}$$

In the cases of $(c,d)=(\bar{\gamma}_N,\infty)$ and $(c,d)=(a_N,b_N)$, the exact values of the integral $J^{(N)}_{c,d}(\theta)$ in (20) can be obtained from the following lemma (refer to Appendix C for the proof).

Lemma 3: For any $\bar{\gamma}_N$ satisfying $a_N\leq\bar{\gamma}_N<b_N$, the exact values of the integrals $J^{(N)}_{\bar{\gamma}_N,\infty}(\theta)$ and $J^{(N)}_{a_N,b_N}(\theta)$ are given by

$$J^{(N)}_{\bar{\gamma}_N,\infty}(\theta)=\sum_{i=1}^{N}\theta^{-i}f^{(N-i)}_{\boldsymbol{a}_0^{N-i}}(\bar{\gamma}_N)e^{-\theta\bar{\gamma}_N}-\mathbb{I}_{\{N\geq 2\}}\sum_{n=0}^{N-2}g^{(n)}_{\bar{\gamma}_N,\infty}(\theta) \tag{21}$$

$$J^{(N)}_{a_N,b_N}(\theta)=\sum_{i=1}^{N}\theta^{-i}\Big[f^{(N-i)}_{\boldsymbol{a}_0^{N-i}}(a_N)e^{-\theta a_N}-f^{(N-i)}_{\boldsymbol{a}_0^{N-i}}(b_N)e^{-\theta b_N}\Big]-\mathbb{I}_{\{N\geq 2\}}\sum_{n=0}^{N-2}g^{(n)}_{a_N,b_N}(\theta). \tag{22}$$

We next show how to apply these preparatory results to evaluate the exact false-alarm probability.

B. False-Alarm Probability

Define $E_N:=\{\Lambda_N\geq b$ and $a<\Lambda_n<b$ for $n\in\aleph_1^{N-1}$ with $N\in\aleph_1^{M-1}\}$ and $E_M:=\{\Lambda_M\geq\gamma$ and $a<\Lambda_n<b$ for $n\in\aleph_1^{M-1}\}$ and let $P_{H_0}(E_N)$ be the probability of event

E_N occurring under H_0. Since the test procedure described in (7)-(9) is the same as that described in (11)-(13), we have

$$P_{H_0}(E_N) = \begin{cases} P_{H_0}(a_i < \xi_i < b_i, i \in \aleph_1^{N-1}; \xi_N \geq b_N), \\ \text{for } N \in \aleph_1^{M-1}; \\ P_{H_0}(a_i < \xi_i < b_i, i \in \aleph_1^{M-1}; \xi_M \geq \bar{\gamma}_M), \\ \text{for } N = M. \end{cases} \tag{23}$$

Clearly, the false-alarm probability α_{ssct} can be written as $\alpha_{\text{ssct}} = \sum_{N=1}^{M} P_{H_0}(E_N)$. The following proposition gives the exact false-alarm probability α_{ssct}.

Proposition 1: The false-alarm probability, α_{ssct}, is given by $\alpha_{\text{ssct}} = \sum_{N=1}^{M} P_{H_0}(E_N)$, where $P_{H_0}(E_N)$ is given by

$$P_{H_0}(E_N) = \begin{cases} A_N \dfrac{b_1 b_N^{N-2}}{(N-1)!}, \ N \in \aleph_1^{P+1}; \\ A_N \Big[f_{\boldsymbol{a}_0^{N-1}}^{(N-1)}(b_{N-1}) - \mathbb{I}_{\{N \geq 3\}} \displaystyle\sum_{n=0}^{N-3} e^{\frac{b_{n+1}}{2}} P_{H_0}(E_{n+1}) \\ \quad \times \dfrac{(b_{N-1} - b_{n+1})^{N-n-1} 2^n}{(N-n-1)!} \Big], \ N \in \aleph_{P+2}^{Q+1}; \\ A_N \Big[f_{\boldsymbol{a}_0^{N-1}}^{(N-1)}(b_{N-1}) - \displaystyle\sum_{n=0}^{N-3} f_{\boldsymbol{\psi}_{n,a_{N-1}}^{N-1}}^{(N-1-n)}(b_{N-1}) \times \\ \quad 2^n e^{\frac{b_{n+1}}{2}} P_{H_0}(E_{n+1}) \Big], \ N \in \aleph_{Q+2}^{M-1}; \\ 2^{-M} J_{\bar{\gamma}_M, \infty}^{(M)}(1/2), \ N = M, \end{cases} \tag{24}$$

where $A_N := 2^{-(N-1)} e^{-b_N/2}$.

Proof: To compute $P_{H_0}(E_N)$, we need to determine the joint PDF of the RVs $(\xi_1, \ldots, \xi_N)$. Let $p_{\boldsymbol{v}|H_0}(v_1, \ldots, v_N|H_0)$ and $p_{\boldsymbol{\xi}|H_0}(\xi_1, \ldots, \xi_N|H_0)$ denote the joint PDFs of the RVs $(v_1, \ldots, v_N)$ and the RVs $(\xi_1, \ldots, \xi_N)$ under H_0, respectively. Recalling that v_i is an exponential RV distributed according to (3), we can write the joint PDF of the RVs $(v_1, \ldots, v_N)$ as $p_{\boldsymbol{v}|H_0}(v_1, \ldots, v_N|H_0) = 2^{-N} e^{-\sum_{i=1}^{N} v_i/2}$. Since $\xi_N = \sum_{i=1}^{N} v_i$, we have $v_1 = \xi_1, v_2 = \xi_2 - \xi_1, \ldots, v_N = \xi_N - \xi_{N-1}$, which yields

$$p_{\boldsymbol{\xi}|H_0}(\xi_1, \xi_2, \ldots, \xi_N|H_0) = p_{\boldsymbol{v}|H_0}(\xi_1, \xi_2 - \xi_1, \ldots, \xi_N - \xi_{N-1}|H_0) = 2^{-N} e^{-\frac{\xi_N}{2}}, \tag{25}$$

where $\xi_0 := 0 \leq \xi_1 \leq \cdots \leq \xi_N$. According to (23) and the definition of $\Upsilon_{b_N, \infty}^{(N)}$, we have

$$P_{H_0}(E_N) = P_{H_0}\Big((\xi_1, \xi_2, \ldots, \xi_N) \in \Upsilon_{b_N, \infty}^{(N)}\Big) = \int \cdots \int_{\Upsilon_{b_N, \infty}^{(N)}} 2^{-N} e^{-\xi_N/2} d\boldsymbol{\xi}_N. \tag{26}$$

Note that each variable ξ_i is lower-bounded by the maximum of a_i and ξ_{i-1}, and is upper-bounded by the minimum of b_i and ξ_{i+1}. Hence, a direct evaluation of (26) is highly complex due to numerous possibilities of upper- and lower-limits of $(\xi_1, \xi_2, \ldots, \xi_N)$ [20].

Nevertheless, in the case of $N \in \aleph_1^{P+1}$, the parameters a_i for $i \in \aleph_1^{N-1}$ are all zeros by the definition of the parameter P. It implies that ξ_i is only lower-bounded by ξ_{i-1} for $i \in \aleph_1^{N-1}$, and accordingly the upper-bound of ξ_i can be readily identified as b_i for $i \in \aleph_1^{N-1}$ [20]. Using [20, Eqs. (16) and (17)] and the fact that $\{b_i\}_{i=1}^{\infty}$ is an arithmetic sequence, we obtain $P_{H_0}(E_N)$ as follows

$$\begin{aligned} P_{H_0}(E_N) &= \int_{\xi_0}^{b_1} d\xi_1 \int_{\xi_1}^{b_2} d\xi_2 \cdots \int_{\xi_{N-2}}^{b_{N-1}} d\xi_{N-1} \int_{b_N}^{\infty} 2^{-N} e^{-\xi_N/2} d\xi_N \\ &= \frac{b_1 b_N^{N-2} e^{-b_N/2}}{2^{N-1}(N-1)!}, \ N \in \aleph_1^{P+1}. \end{aligned} \tag{27}$$

We now consider the case of $N \in \aleph_{P+2}^{M-1}$. Since $\xi_N \in [b_N, \infty)$ and $b_N > b_{N-1}$, the upper-limit of ξ_{N-1} is actually b_{N-1} irrespective of ξ_N. From (18), we can write (26) as

$$\begin{aligned} P_{H_0}(E_N) &= \int_{b_N}^{\infty} 2^{-N} e^{-\xi_N/2} d\xi_N \cdot \int \cdots \int_{\Omega^{(N-1)}} d\boldsymbol{\xi}_{N-1} \\ &= 2^{-(N-1)} e^{-b_N/2} I^{(N-1)} \end{aligned} \tag{28}$$

with $N \in \aleph_{P+2}^{M-1}$. By applying (18), $P_{H_0}(E_N)$ for $N \in \aleph_{P+2}^{Q+1}$ and $N \in \aleph_{Q+2}^{M-1}$ in (24) can be readily obtained. We next compute $P_{H_0}(E_M)$. Since $\bar{\gamma}_M \in (a_M, b_M)$, the upper-limit of ξ_{M-1} depends on both ξ_M and b_{M-1}. Thus, the integrals $\int d\xi_M$ and $\int \cdots \int d\boldsymbol{\xi}_{M-1}$ are not separable. It is clear from Lemma 3 that $P(E_M|H_0)$ can be obtained from $J_{\bar{\gamma}_M, \infty}^{(M)}(\theta)$ by setting $\theta = 1/2$ and $N = M$ in (21). Hence, we have

$$\begin{aligned} P_{H_0}(E_M) &= P_{H_0}\Big((\xi_1, \ldots, \xi_M) \in \Upsilon_{\bar{\gamma}_M, \infty}^{(M)}\Big) \\ &= \int \cdots \int_{\Upsilon_{\bar{\gamma}_M, \infty}^{(M)}} 2^{-M} e^{-\xi_M/2} d\boldsymbol{\xi}_M = 2^{-M} J_{\bar{\gamma}_M, \infty}^{(M)}\big(1/2\big). \end{aligned} \tag{29}$$

From (27), (28), and (29), we can conclude the proof. ■

Remark 1: It is worth noting that the false-alarm probability evaluation problem for SSCT is similar to the well-known OC evaluation problem in T-SLT for exponential distribution. Woodall and Kurkjian solved the exact OC problem for T-SLT with exponential distribution [20]. Nevertheless, the Woodall-Kurkjian solution to the exact OC problem is not applicable to evaluate ASN [21]. More precisely, it is not applicable to evaluate (29) directly. In the preceding proof, we propose a different method to derive the exact false-alarm probability α_{ssct}. With slight modifications, this method can also be used to evaluate ASN for T-SLT in the exponential case.

C. Misdetection Probability

We now show how to evaluate the misdetection probability β_{ssct} for SSCT. Evaluating β_{ssct} is more difficult than evaluating α_{ssct}. The main reason is that to compute β_{ssct}, one needs to know $p_{H_1}(v_i)$. However, computing $p_{H_1}(v_i)$ is intractable except when primary signal samples have the constant-modulus property, i.e., $|s_i|^2 = \sigma_s^2$. We next show that at a relatively low detection SNR level, the misdetection probability obtained by assuming constant-modulus primary signals can be used to well approximate the actual β_{ssct}. Our arguments are primarily based on the following two properties of SSCT.

The first property shows that as N approaches infinity, the distribution of the test statistic ξ_N in SSCT converges to a normal distribution that is independent of a specific choice of $\lambda_1, \lambda_2, \ldots, \lambda_N$.

Property 1: The statistical distribution of ξ_N converges to a normal distribution given by

$$\xi_N \sim \begin{cases} \mathcal{N}(2N, 4N), & \text{under } H_0, \\ \mathcal{N}\big(2N(1+\mathtt{SNR}_m), 4N(1+2\mathtt{SNR}_m)\big), & \text{under } H_1, \end{cases}$$

as N approaches infinity.

The property can be readily proved by using CLT [22]. However, unlike energy detection, this property alone is not sufficient to explain that the constant-modulus assumption is valid in approximating β_{ssct}. This is because each ξ_N for $N = 1, \ldots, M$, including small values of N, may potentially affect the value of β_{ssct}. To complete our argument, we first present the following definitions. Let $\tilde{\xi}_i$ denote the test statistic using the constant-modulus assumption, i.e., $|s_i|^2 = \sigma_s^2$. Define $\varrho_N := b_N$ for $N \in \aleph_1^{M-1}$ and $\varrho_M := \bar{\gamma}_M$ for $N = M$. Let F_N and $\tilde{F}_N$ denote the events that $\xi_N \geq \varrho_N$, and $a_i < \xi_i < b_i$ for $i \in \aleph_1^M$, and $\tilde{\xi}_N \geq \varrho_N$ and $a_i < \tilde{\xi}_i < b_i$ for $i \in \aleph_1^M$, respectively. Let $P_{H_1}(F_N)$ and $P_{H_1}(\tilde{F}_N)$ denote the probabilities of the events F_N and $\tilde{F}_N$ under H_1. Let $\tilde{\beta}_{\text{ssct}}$ denote the misdetection probability obtained by assuming constant-modulus signals with average symbol energy σ_s^2, i.e., $|s_i|^2 = \sigma_s^2$. As clear from their definitions, we have $\beta_{\text{ssct}} = \sum_{N=1}^{M} P_{H_1}(F_N)$ and $\tilde{\beta}_{\text{ssct}} = \sum_{N=1}^{M} P_{H_1}(\tilde{F}_N)$.

Let $\mathcal{A}_N^{l_N}$ denote the event that $a_i < \xi_i < b_i,\ i \in \aleph_1^{l_N}$ for some integer $l_N \in \aleph_1^N$, and let $\tilde{\mathcal{A}}_N^{l_N}$ denote its counterpart for the constant-modulus case. Let $\mathcal{B}_N^{l_N}$ denote the event that $\xi_N \geq \varrho_N$ and $a_i < \xi_i < b_i,\ i \in \aleph_{l_N+1}^N$ and let $\tilde{\mathcal{B}}_N^{l_N}$ denote its counterpart in the constant-modulus case. We now present the second property (refer to Appendix D for the proof).

Property 2: For any $\epsilon > 0$, if for each N, there exists a positive integer $l_N \in \aleph_1^N$ such that $P_{H_1}(\mathcal{A}_N^{l_N}) \geq 1 - \epsilon/(3M)$, $P_{H_1}(\tilde{\mathcal{A}}_N^{l_N}) \geq 1 - \epsilon/(3M)$, and $|P_{H_1}(\mathcal{B}_N^{l_N}) - P_{H_1}(\tilde{\mathcal{B}}_N^{l_N})| < \epsilon/(3M)$, then $|\beta_{\text{ssct}} - \tilde{\beta}_{\text{ssct}}| \leq \epsilon$.

Relying on these two properties, we provide an outline of our arguments. To achieve a high detection accuracy at a low SNR level, ASN and M are typically quite large. When the sample index N is relatively small, it is highly unlikely that the test statistics ξ_N and $\tilde{\xi}_N$ cross either of the two boundaries. In such a situation, there exists some integer l_N such that $P_{H_1}(\mathcal{A}_N^{l_N})$ and $P_{H_1}(\tilde{\mathcal{A}}_N^{l_N})$ are fairly close to 1 whereas $P_{H_1}(\mathcal{B}_N^{l_N})$ and $P_{H_1}(\tilde{\mathcal{B}}_N^{l_N})$ are fairly close to 0. Hence, the conditions in Property 2 can be easily satisfied. On the other hand, when N is relatively large, one can find a sufficiently large l_N such that $P_{H_1}(\mathcal{A}_N^{l_N})$ and $P_{H_1}(\tilde{\mathcal{A}}_N^{l_N})$ are fairly close to one while $|P_{H_1}(\mathcal{B}_N^{l_N}) - P_{H_1}(\tilde{\mathcal{B}}_N^{l_N})|$ is sufficiently small due to Property 1 guaranteed by the CLT. Collectively, at a low detection SNR level, $\tilde{\beta}_{\text{ssct}}$ evaluated under the constant-modulus assumption is a close approximation of β_{ssct}. Therefore, we will focus on the case in which all λ_i's are equal to a constant $\lambda := 2|h|^2\sigma_s^2/\sigma_w^2 = 2\mathtt{SNR}_m$.

Recall that under H_1, v_i is a non-central chi-square RV, whose PDF involves the zeroth-order modified Bessel function of the first kind as given in (4). Hence, it is mathematically intractable to evaluate $\tilde{\beta}_{\text{ssct}}$ by applying the computational approach used in Section IV-B. To obtain $\tilde{\beta}_{\text{ssct}}$, we apply a numerical integration algorithm proposed in [23].

Defining $u_i = v_i - \bar{\Delta}$, we express $\bar{\Lambda}_N$ in (10) as $\bar{\Lambda}_N = \sum_{i=1}^{N} u_i$. Clearly, the PDF of u_i under hypothesis H_1 can be rewritten as $p_{H_1}(u_i) = \frac{1}{2}e^{-(u_i+\bar{\Delta}+\lambda)} I_0\Big(\sqrt{\lambda(u_i+\bar{\Delta})}\Big), u_i > -\bar{\Delta}$. Note that SSCT observes at most M samples before making a decision. Let t_k denote $\bar{\Lambda}_{M-k}$. We also use $G_k(t_k)$ to denote the conditional misdetection probability conditioning on the follow event: the first $(M-k)$ samples have been collected, the present observation value is $t_k = \bar{\Lambda}_{M-k}$, and the test statistic of the previous $(M-k-1)$ samples has not crossed either the upper- or lower-boundary. When $\bar{a} < t_k < \bar{b}$ for $k = 1, \ldots, M$, SSCT needs to collect an additional sample (the $(M-k+1)$th sample). For notation simplicity, we use u to denote the next observed value of u_i. We can write the conditional probability $G_k(t_k|u)$ as

$$G_k(t_k|u) = \begin{cases} 0 & \text{if } u > \bar{b} - t_k \\ 1 & \text{if } u < \bar{a} - t_k \\ G_{k-1}(t_k + u) & \text{if } \bar{a} - t_k \leq u \leq \bar{b} - t_k. \end{cases} \tag{30}$$

Using (30), we can compute $G_k(t_k)$ as

$$G_k(t_k) = \int_{-\infty}^{\bar{a}-t_k} p_{H_1}(u)du + \int_{\bar{a}-t_k}^{\bar{b}-t_k} G_{k-1}(t_k+u)p_{H_1}(u)du \tag{31}$$

for $k = 1, \cdots, M$ with the following initial condition: $G_0(t_0) = 0$ if $t_0 \geq \bar{\gamma}$ and $G_0(t_0) = 1$, otherwise. Note that $G_M(0)$ is indeed the misdetection probability $\tilde{\beta}_{\text{ssct}}$. By applying the backward recursion algorithm described above, the value of $G_M(0)$ is obtained.

Remark 2: Even though evaluation procedures of false-alarm and misdetection probabilities described in this section are complicated, they are performed in an *off-line* basis and are only used to determine design parameters such as thresholds a, b, γ, and M. Alternatively speaking, evaluation procedures of false-alarm and misdetection probabilities are related to the designs of the sensing algorithms. Nonetheless, they are not the part of the SSCT-based sensing process and thus the complexity of these evaluation procedures is not related to the implementation complexity of SSCT.

V. Evaluation of the Average Sample Number

In this section, we discuss how to evaluate ASN of the proposed algorithm. Let N_s denote the number of samples required to yield a decision. Clearly, N_s is a RV in SSCT, and its mean value is ASN, which can be written as

$$E(N_s) = E_{H_0}(N_s)\pi_0 + E_{H_1}(N_s)\pi_1 \tag{32}$$

where $E_{H_i}(N_s)$ denotes ASN under H_i, and π_i denotes the *priori* probability of hypothesis H_i, for $i = 0, 1$.

According to (7)–(9), we have $1 \leq N_s \leq M$. Hence, we can express $E_{H_i}(N_s)$ as

$$E_{H_i}(N_s) = \sum_{N=1}^{M} N P_{H_i}(N_s = N),\ i = 0, 1 \tag{33}$$

where $P_{H_i}(N_s = N)$ is the probability that the detector makes a decision at the Nth sample under H_i. We now need to determine $P_{H_i}(N_s = N)$. Let $\mathcal{C}_N$ denote the event that the test statistics $(\xi_1, \xi_2, \ldots, \xi_N)$ do not cross either the upper or lower boundary before or at the Nth sample, i.e., $\mathcal{C}_N = \{(\xi_1, \xi_2, \ldots, \xi_N) \in \Upsilon_{a_N, b_N}^{(N)}\}$ for $N \in \aleph_1^M$. For notional

convenience, let us define $\mathcal{C}_0$ as a universe set. Hence, we have $P(\mathcal{C}_0) = 1$. The test procedure described in (11)-(13) implies that $P_{H_i}(N_s = N),\ i = 0, 1$ can be obtained as

$$P_{H_i}(N_s = N) \overset{(a)}{=} P_{H_i}\big(\mathcal{C}_{N-1}\big) - P_{H_i}\big(\mathcal{C}_N\big),\ N \in \aleph_1^{M-1} \quad (34)$$

$$P_{H_i}(N_s = M) \overset{(b)}{=} P_{H_i}\big(\mathcal{C}_{M-1}\big), \qquad N = M \quad (35)$$

where $P_{H_i}(\mathcal{C}_{N-1})$ and $P_{H_i}(\mathcal{C}_N)$ in (a) denote the respective probabilities of the following events: under H_i, the test statistic does not cross either the upper- or lower-boundary before or at the $(N-1)$th sample and the Nth sample for $N \in \aleph_1^{M-1}$, and $P_{H_i}(\mathcal{C}_{M-1})$ in (b) denotes the probability of the following event: under H_i, the test statistic does not cross either upper- or lower-boundary before or at the $(M-1)$th sample. Clearly, using (34) and (35), we can express (33) as

$$E_{H_i}(N_s) = \sum_{N=1}^{M-1} N\Big(P_{H_i}(\mathcal{C}_{N-1}) - P_{H_i}(\mathcal{C}_N)\Big) + MP_{H_i}(\mathcal{C}_{M-1}) = 1 + \sum_{N=1}^{M-1} P_{H_i}(\mathcal{C}_N). \quad (36)$$

Applying Lemma 3, (25), (34), and (35), we obtain $P_{H_0}\big(\mathcal{C}_N\big) = 2^{-N} J^{(N)}_{a_N, b_N}(1/2),\ N \in \aleph_1^{M-1}$. Hence, according to (36), we have

$$E_{H_0}(N_s) = 1 + \sum_{N=1}^{M-1} 2^{-N} J^{(N)}_{a_N, b_N}(1/2). \quad (37)$$

We next show how to obtain $P_{H_1}(\mathcal{C}_N)$, or equivalently how to obtain $P_{H_1}(\mathcal{C}_N^c)$. To compute $P_{H_1}(\mathcal{C}_N^c)$, we apply a similar computation method to the one used in computing the misdetection probability. It should be noted that $\mathcal{C}_N^c$ indicates the following event: under H_1, the test procedure given in (11)-(13) stops before or at the Nth sample, i.e., the test statistic crosses either the upper or lower boundary before or at the Nth sample. With a slight abuse of notation, we rewrite $G_k(t_k)$ as $G_k(t_k, \bar{\gamma})$. We use V_N to denote the following event: the test statistic crosses the lower boundary before or at the Nth sample under H_1, and we use U_N to denote the following event: the test statistic *does not* cross the upper-boundary before or at the Nth sample under H_1. By the definitions of V_N, U_N, and G_N, we have $P_{H_1}(V_N) = G_N(0, \bar{a})$ and $P_{H_1}(U_N) = G_N(0, \bar{b})$. Clearly, we can write $P_{H_1}(\mathcal{C}_N^c)$ as

$$P_{H_1}\big(\mathcal{C}_N^c\big) = G_N(0, \bar{a}) + 1 - G_N(0, \bar{b}) \quad (38)$$

where $G_N(t, \bar{a})$ and $G_N(t, \bar{b})$ can be obtained by applying (31) recursively. From (38), we have $P_{H_1}(\mathcal{C}_N) = G_N(0, \bar{b}) - G_N(0, \bar{a})$. According to (36), we have

$$E_{H_1}(N_s) = 1 + \sum_{N=1}^{M-1} (G_N(0, \bar{b}) - G_N(0, \bar{a})). \quad (39)$$

In the following proposition, we present the ASN of SSCT.

Proposition 2: The ASN of SSCT can be obtained as

$$E(N_s) = \pi_0\Big(1 + \sum_{N=1}^{M-1} 2^{-N} J^{(N)}_{a_N, b_N}(1/2)\Big) + \pi_1\Big(1 + \sum_{N=1}^{M-1} (G_N(0, \bar{b}) - G_N(0, \bar{a}))\Big).$$

TABLE I
SCCT VERSUS ENERGY DETECTION

$\mathtt{SNR}_m$ (dB)	0	-5	-10	-15
$\bar{\gamma}$	-8.5	-5.69	-4	-1.897
$\bar{b}$	27	35.32	69.30	158.47
$\bar{\Delta}$	3	2.316	2.100	2.032
α_{ssct} (Monte Carlo)	0.011	0.055	0.103	0.153
α_{ssct} (Numerical)	0.011	0.055	0.103	0.153
α_{ed} (Energy Detect.)	0.011	0.055	0.101	0.150
β_{ssct} (Monte Carlo)	0.008	0.046	0.099	0.154
β_{ssct} (Numerical)	0.008	0.047	0.100	0.156
β_{ed} (Energy Detect.)	0.008	0.046	0.096	0.149
ASN (Monte Carlo)	26	95	509	3154
ASN (Numerical)	26	96	515	3185
M (Energy Detect.)	40	140	730	4450
Efficiency η	35%	32%	30%	29%

Proof: The proof follows immediately from (32), (37), and (39). ■

VI. NUMERICAL EXAMPLES

In this section, we present several numerical examples to test the SSCT algorithm and validate the results obtained in Sections IV and V. In these examples, the parameter $\bar{\Delta}$ is selected to be $2 + \mathtt{SNR}_m$. With this choice of $\bar{\Delta}$, we have $E_{H_0}(|r_i|^2 - \Delta) = E_{H_1}(|r_i|^2 - \Delta) = -\sigma_s^2/2$, and thus $E_{H_0}(\Lambda_N) = -E_{H_1}(\Lambda_N)$ for every $N \geq 0$. It implies that statically, the Test Statistic Λ_N moves the same distance on average upwards or downwards at each step. Roughly speaking, such choice of the parameter Δ will lead to an approximately same average sample number under H_0 or H_1. In the first three test examples, we select the parameter M to be the minimum required sample number $M_{\text{ed}}^{\min}$ for energy detection to achieve the target false-alarm and misdetection probabilities, and we choose $\bar{a}$ to be $-\bar{b}$. In all test examples, the channel gains $|h|$ are equal to one, and primary signals are constant-modulus quadrature phase shift-keying (QPSK) signals except for Test Example 2, in which the modulation formats of the primary signals are explicitly stated. Following conventional terminology in the sequential detection, we define the efficiency of SSCT as $\mathcal{E}_{\text{SSCT}} = 1 - \text{ASN}_{\text{SSCT}}/M_{\min}^{ed}$.

Test Example 1: Table I lists false-alarm and misdetection probabilities and ASN for different $\mathtt{SNR}_m$ for both SSCT and energy detection. For $\mathtt{SNR}_m = 0$, -5, -10, and -15 dB, we select the corresponding truncation sizes to be the minimum sample sizes required by energy detection to achieve $(\bar{\alpha}_{\text{ed}}, \bar{\beta}_{\text{ed}}) = (0.01, 0.01)$, $(0.05, 0.05)$, $(0.1, 0.1)$, and $(0.15, 0.15)$, respectively. The parameters $\bar{b}$, $\bar{\Delta}$ and $\bar{\gamma}$ are given in the table. Table I shows that while maintaining a comparable detection performance, SSCT is capable of achieving about $29\% \sim 35\%$ savings in terms of the average sensing time as compared with energy detection. We use an abbreviation, Numerical, in the parenthesis, to indicate the results obtained by either the exact formula (24) for false-alarm probabilities or by the numerical integration algorithm for misdetection probabilities. As can be seen from the table, the results obtained by the numerical approach and those obtained by the Monte-Carlo simulation are fairly close.

Test Example 2: In this example, we assume that primary signals are square 64-quadrature amplitude modulation

TABLE II
DETECTION PERFORMANCE WITHOUT KNOWING MODULATION TYPES OF THE PRIMARY SIGNALS

$\mathtt{SNR_m}$ (dB)	0	-5	-10	-15
β_{ssct} (QPSK,Monte Carlo)	0.008	0.046	0.099	0.154
β_{ssct} (QPSK,Numerical)	0.008	0.047	0.100	0.156
β_{ed} (QPSK,Energy Detect.)	0.008	0.046	0.096	0.149
β_{ssct} (64-QAM,Monte Carlo)	0.012	0.048	0.099	0.154
β_{ssct} (64-QAM,Numerical)	0.012	0.050	0.103	0.157
β_{ed} (64-QAM,Energy Detect.)	0.012	0.047	0.096	0.149
ASN (QPSK,Monte Carlo)	26	95	509	3154
ASN (QPSK,Numerical)	26	96	515	3185
ASN (64-QAM,Monte Carlo)	26	95	509	3154
ASN (64-QAM,Numerical)	26	96	514	3190

TABLE III
MISMATCH BETWEEN $\mathtt{SNR_m}$ AND $\mathtt{SNR_o}$ ($\mathtt{SNR_m} = -15$ dB)

SNR_o (dB)	-12	-13	-14	-15
β_{ssct} (Monte Carlo)	0.0018	0.0153	0.0629	0.154
β_{ssct} (Numerical)	0.0017	0.0151	0.0628	0.156
β_{ed} (Energy Detect.)	0.0012	0.0131	0.0584	0.149
ASN (Monte Carlo)	2425	2686	2948	3154
ASN (Numerical)	2499	2769	3035	3185
M (Energy Detect.)	4450	4450	4450	4450
$\mathcal{E}_{ssct}$	46%	40%	34%	29%

(QAM) signals with $\sigma_s^2 = 10^{\mathtt{SNR}_m/10}\sigma_w^2$. Table II lists misdetection probabilities and ASN for SSCT and energy detection when $\mathtt{SNR}_m = 0$, -5, -10, and -15 dB. To demonstrate the fact that SSCT does not rely on the knowledge of the modulation format of primary signals, we determine the parameters $\bar{a}$, $\bar{b}$, $\bar{\gamma}$, $\bar{\Delta}$, and M in SSCT, by applying QPSK signals with average symbol energy $\sigma_s^2 = 10^{\text{SNR}_m/10}\sigma_w^2$ while we apply these design parameters determined by QPSK primary signals to detect the i.i.d. 64-QAM signal samples, which are drawn from 64-QAM constellation points with equal probability. It is evident from the table that the misdetection probabilities obtained in the 64-QAM case and the QPSK case match well except for the case of $\mathtt{SNR}_m = 0$ dB (correspondingly, $M = 40$). This is because M is not large enough to neglect errors caused by using the CLT approximation. However, the energy detection and SSCT sensing algorithms have a similar amount of approximation error in terms of the misdetection probability.

Test Example 3: In this example, we study the detection performance of SSCT and the energy detection when there is a mismatch between $\mathtt{SNR}_o$ and $\mathtt{SNR}_m$. For $\mathtt{SNR}_o = -12$, -13, -14 dB, and $\mathtt{SNR}_m = -15$ dB, the false-alarm and misdetection probabilities and ASN are listed in Table III. We choose the parameters for SSCT and energy detection such that target false-alarm and misdetection probabilities are around $(0.15, 0.15)$ at $\mathtt{SNR}_m = -15$ dB. As can be seen from the table, for both SSCT and energy detection, the misdetection probabilities decrease as $\mathtt{SNR}_o$ increases, while the false-alarm probabilities keep the same. It is clear from the table that the false-alarm and misdetection $(\alpha_{\text{ssct}}, \beta_{\text{ssct}})$ satisfy the target detection error probability requirements. As the mismatch between $\mathtt{SNR}_o$ and $\mathtt{SNR}_m$ increases, the efficiency of SSCT increases from 29% to 46%. This implies that compared with the energy detection, SSCT offers an additional flexibility in striking a desirable sensing time and detection performance tradeoff in the SNR mismatch case.

TABLE IV
IMPACTS OF TRUNCATION SIZE M ($\mathtt{SNR_o} = -5$ dB, MONTE CARLO SIMULATION)

M	$\bar{a}$	b	$\bar{\gamma}$	ASN	T_p	η
$M = 140$	-35.32	35.32	-5.69	95.4	26.8%	32%
$M = 160$	-28.95	23.16	-5.50	76.7	9.2%	45%
$M = 180$	-27.33	21.54	-6.00	73.1	5.1%	48%
$M = 200$	-26.40	20.85	-6.32	71.2	3.0%	49%
$M = 500$	-25.48	19.69	-6.32	68.8	0.005%	51%
$M = 1000$	-25.42	19.63	-6.32	68.6	0	51%
SPRT	–	–	–	67.9	0	52%

Test Example 4: Let T_p be the probability of the event that SSCT ends at the Mth sample (i.e., the test is truncated at the Mth sample). Table IV lists T_p, the ASN, and the efficiency of SSCT for various selected combinations of M, $\bar{a}$, $\bar{b}$, and $\bar{\gamma}$ at $\mathtt{SNR}_m = -5$ dB to achieve target $(\bar{\alpha}_{\text{ssct}}, \bar{\beta}_{\text{ssct}}) = (0.055, 0.046)$. The results shown in the table are obtained by Monte Carlo simulation. To achieve roughly the same false-alarm and misdetection probabilities, the sample size for energy detection is chosen to be 140. As can be seen from this table, the efficiency of SSCT increases as the truncated size M increases but the pace of the improvement is diminishing. Table IV also lists the efficiency of the non-truncated SPRT-based sensing algorithm presented in Section II-B2. It is clear from the table that as the truncated size M increases, the efficiency of SSCT comes fairly close to the one achieved by the *non-truncated* SPRT-based sensing algorithm.

VII. CONCLUSION

In CR networks, stringent requirements on the secondary and opportunistic access to the licensed spectrum necessitate the need to develop a spectrum sensing algorithm that is able to quickly detect weak primary signals with high accuracy in a non-coherent fashion. Motivated by this need, we have proposed a sequential sensing algorithm that possesses several desirable features suitable for CR networks. To efficiently and accurately obtain major performance benchmarks of our sensing algorithm, we have derived an exact formula for the false-alarm probability and have developed numerical integration algorithms to compute the misdetection probability and ASN.

There are several potential extensions of this work that deserve further exploration. First, our approach to determine the design parameters such as the thresholds and the truncated size follows the original Wald's approach in the sense that the cost of observations as well as the cost of the false-alarm and misdetection events have not been considered. A Bayesian formulation of SSCT can be an interesting extension. Second, this work assumes the perfect knowledge on the noise power at SU, which might be difficult to acquire in practice. The effect of noise power uncertainty [15] on SSCT is worth investigating. Third, another extension of this work is to study sensing-throughput tradeoffs [1] for SSCT.

APPENDIX A
PROOF OF LEMMA 1

We prove the lemma by induction. It is obvious from (14) that (15) holds for $k = 1$. Now suppose that (15) and (16)

hold for the case of $k-1$. By definition and the induction assumption for $k-1$, we have

$$\begin{aligned} & f_{\boldsymbol{\chi}_k}^{(k)}(\xi) \\ &= \int_{\chi_k}^{\xi} \Big(\sum_{i=0}^{k-2} \frac{f_i^{(k-1)}}{(k-1-i)!} (\xi_{k-1} - \chi_{i+1})^{k-1-i} + f_{k-1}^{(k-1)} \Big) d\xi_{k-1} \\ &= \sum_{i=0}^{k-1} \frac{f_i^{(k-1)}}{(k-i)!} (\xi - \chi_{i+1})^{k-i} - \sum_{i=0}^{k-2} \frac{f_i^{(k-1)}}{(k-i)!} (\chi_k - \chi_{i+1})^{k-i}. \end{aligned} \tag{40}$$

Clearly, comparing (15) with (40), we can readily conclude the recurrence relation given in (16). In particular, when $\chi_1 = \chi_2 = \ldots = \chi_k$, all coefficients $f_i^{(k)}$ except $f_0^{(k)}$ are zeros and hence (17) follows immediately.

Since the differential property can be proved in a straightforward manner, we omit the proof. We next prove the scaling property by induction. When $k=1$, we have

$$f_{t\boldsymbol{\chi}_1}^{(1)}(t\xi) = \int_{t\chi_1}^{t\xi} d\xi_1 = t(\xi - \chi_1) = t f_{\boldsymbol{\chi}_1}^{(1)}(\xi).$$

Hence, the scaling property holds for $k=1$. We now suppose that the property holds for $k = n-1$. Applying the induction assumption and a substitution $t\xi_n = u$, we can rewrite the integral $f_{\boldsymbol{\chi}_n}^{(n)}(\xi)$ as

$$\begin{aligned} f_{\boldsymbol{\chi}_n}^{(n)}(\xi) &= \int_{\chi_n}^{\xi} f_{\boldsymbol{\chi}_{n-1}}^{(n-1)}(\xi_n) d\xi_n = \int_{\chi_n}^{\xi} t^{-(n-1)} f_{t\boldsymbol{\chi}_{n-1}}^{(n-1)}(t\xi_n) d\xi_n \\ &= t^{-n} \int_{t\chi_n}^{t\xi} f_{t\boldsymbol{\chi}_{n-1}}^{(n-1)}(u) du = t^{-n} f_{t\boldsymbol{\chi}_n}^{(n)}(t\xi). \end{aligned}$$

Hence, the scaling property holds for $k=n$. This concludes the proof. The shift property can be proved in a similar manner and thus the proof is omitted. ■

APPENDIX B
PROOF OF LEMMA 2

Recall that $\xi_N = \sum_{i=1}^{N} v_i$ with $v_i = 2|r_i|^2/\sigma_w^2$. Hence, $(\xi_1, \xi_2, \ldots, \xi_N)$ is a non-decreasing sequence, i.e., $\xi_0 \le \xi_1 \le \cdots \le \xi_N$. Fig. 3(a) plots the parameter ξ_N versus the sample index N. It is clear from its definition that the region $\Omega^{(N)}$ contains all possible sequences $(\xi_1, \xi_2, \ldots, \xi_N)$ (called paths hereafter) satisfying $\xi_0 \le \xi_1 \le \ldots \le \xi_N$ and $0 \le a_i < \xi_i < b_i$. Hence, the ith component of each path $(\xi_1, \xi_2, \ldots, \xi_N)$ in $\Omega^{(N)}$ is lower-bounded by the maximum of ξ_{i-1} and a_i, and is upper-bounded by the minimum of ξ_{i+1} and b_i. The direct computation of $I^{(N)}$ is highly complex [20] due to numerous possibilities for lower- and upper-limits in the integral $I^{(N)}$. Considering the fact that $I^{(N)}$ can be readily computed if either the lower- or upper-limit is a constant, we express $\Omega^{(N)}$ into an equivalent set, over which the integration can be readily computed in a recursive fashion, thereby obviating the need to exhaustively enumerate these possibilities.

Let $\phi_i,\ i \in \aleph_1^N$, denote a sequence of real numbers with $0 \le \phi_1 \le \ldots \le \phi_N$. Let us first define the following set,

$$\begin{aligned} \Pi_{\boldsymbol{\phi}_n^N}^{(N-n)} = \{ & (\xi_{n+1}, \xi_{n+2}, \ldots, \xi_N) : 0 \le \xi_{n+1} \ldots \le \xi_N; \phi_i < \\ & \xi_i \le \xi_{i+1}, i \in \aleph_{n+1}^{N-1}; \phi_N < \xi_N < b_N \} \end{aligned} \tag{41}$$

where $\boldsymbol{\phi}_n^N := [\phi_{n+1}, \ldots, \phi_N]$ is an $(N-n)$-dimensional real vector with the ith entry of the vector $\boldsymbol{\phi}_n^N$ being the lower bound of ξ_{n+i} for $i \in \aleph_1^{N-n}$. We next define the following non-overlapping subsets of $\Pi_{\boldsymbol{a}_0^N}^{(N)}$,

$$\begin{aligned} \Xi_n^{(N)} := \{ & (\xi_1, \ldots, \xi_N) : (\xi_1, \ldots, \xi_N) \in \Pi_{\boldsymbol{a}_0^N}^{(N)}, \\ & a_i < \xi_i < b_i, i \in \aleph_1^n; b_{n+1} \le \xi_{n+1} \le \xi_{n+2} \} \end{aligned} \tag{42}$$

where $n \in \aleph_0^{N-2}$. As can be seen from Figs. 3(b) and 3(c), $\Pi_{\boldsymbol{a}_0^N}^{(N)}$ contains all possible paths, $(\xi_1, \xi_2, \ldots, \xi_N)$, which are lower-bounded by $(a_1, a_2, \ldots, a_N)$ and upper-bounded by $(\xi_2, \xi_3, \ldots, \xi_N, b_N)$, whereas $\Xi_n^{(N)}$ for $n \in \aleph_0^{N-2}$ contains all possible paths $(\xi_1, \xi_2, \ldots, \xi_N)$ having the property that the first n variables lie in the set $\Omega^{(n)}$, i.e., $(\xi_1, \ldots, \xi_n) \in \Omega^{(n)}$, and the $(n+1)$th variable ξ_{n+1} excesses the upper slant line, i.e., $\xi_{n+1} \ge b_{n+1}$. Again, it is clear from its definition that the set $\Omega^{(N)}$ is equal to the difference between the set $\Pi_{\boldsymbol{a}_0^N}^{(N)}$ and the union of $\Xi_n^{(N)}$ for $n \in \aleph_0^{N-2}$, i.e., $\Omega^{(N)} = \Pi_{\boldsymbol{a}_0^N}^{(N)} \cap \big(\cup_{n=0}^{N-2} \Xi_n^{(N)} \big)^c$. Thus, it follows from (18) that

$$I^{(N)} = \int_{\Pi_{\boldsymbol{a}_0^N}^{(N)}} \cdots \int d\boldsymbol{\xi}_N - \sum_{n=0}^{N-2} \int_{\Xi_n^{(N)}} \cdots \int d\boldsymbol{\xi}_N. \tag{43}$$

We now evaluate two terms on the right-hand side (RHS) of (43). It is clear from (14) and (41) that the first term on the RHS of (43) is nothing but $f_{\boldsymbol{a}_0^N}^{(N)}(b_N)$. We next take a close look at the second term. The evaluation of the second term is categorized into the following two cases:

- Case 1: $N \le Q$: In this case, we have $b_{n+1} > b_1 \ge a_n$ for any $n \in \{1, \ldots, N\}$. It implies from (42) that we can express $\Xi_n^{(N)}$ as $\Xi_n^{(N)} = \Omega^{(n)} \times [b_{n+1}, \xi_{n+2}] \times \cdots \times [b_{n+1}, \xi_N] \times [b_{n+1}, b_N]$ for $n = 0, \ldots, N-2$ where $\Omega^{(0)} := \emptyset$. According to (41), we have

$$\Xi_n^{(N)} = \Omega^{(n)} \times \Pi_{b_{n+1}\mathbf{1}_{N-n}}^{(N-n)},\ n \in \aleph_0^{N-2}. \tag{44}$$

  Since $\xi_{n+1} > b_{n+1} > b_n > \xi_n$, the integral over $\Omega^{(n)}$ and that over $\Pi_{b_{n+1}\mathbf{1}_{N-n}}^{(N-n)}$ are separable. Hence, relying on (19), (42) and (44), we have

$$\begin{aligned} & \int_{\Xi_n^{(N)}} \cdots \int d\boldsymbol{\xi}_N = \int_{\Pi_{b_{n+1}\mathbf{1}_{N-n}}^{(N-n)}} \cdots \int d\xi_{n+1} \cdots d\xi_N \times \\ & \int_{\Omega^{(n)}} \cdots \int d\xi_1 \cdots d\xi_n = f_{b_{n+1}\mathbf{1}_{N-n}}^{(N-n)}(b_N) I^{(n)}. \end{aligned} \tag{45}$$

- Case 2: $N \ge Q+1$: The proof in this case follows the same line of argument as that in the previous case. The key difference is that because $N \ge Q+1$, some a_n may be larger than b_{n+1}, as depicted in Fig. 3(d). To be specific, from the definition of Q, we have $a_Q \le b_1 < a_{Q+1}, \ldots, a_{Q+n} \le b_{n+1} < a_{Q+n+1}, \ldots, a_N \le b_{N-Q+1} < a_{N+1}$.

  1) For $n \in \aleph_0^{N-Q-1}$, we have $\Xi_n^{(N)} = \Omega^{(n)} \times \underbrace{[b_{n+1}, \xi_{n+2}] \times \cdots \times [b_{n+1}, \xi_{n+Q+1}]}_{Q} \times \underbrace{[a_{Q+n+1}, \xi_{Q+n+2}] \times \cdots \times [a_{N-1}, \xi_N] \times [a_N, b_N]}_{N-Q-n}$.

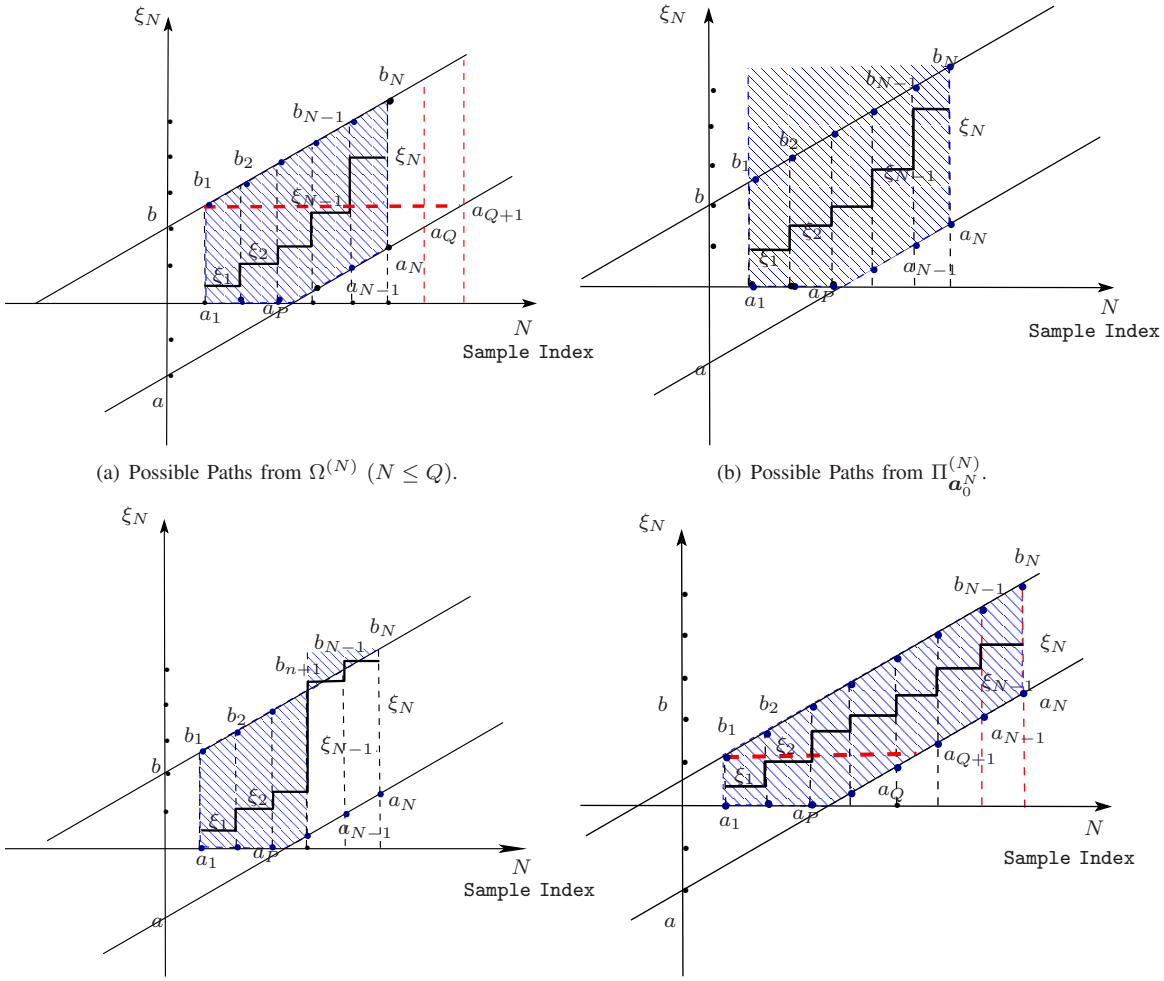

(a) Possible Paths from $\Omega^{(N)}$ $(N \leq Q)$.

(b) Possible Paths from $\Pi^{(N)}_{\boldsymbol{a}_0^N}$.

(c) Possible Paths from $\Xi^{(N)}_n$.

(d) Possible Paths from $\Omega^{(N)}$ $(N > Q)$.

Fig. 3. An illustration for Proof of Lemma 2.

Equivalently, $\Xi^{(N)}_n = \Omega^{(n)} \times \Pi^{(N-n)}_{\boldsymbol{\psi}^N_{n,a_N}}$ with $\boldsymbol{\psi}^N_{n,a_N} = [\underbrace{b_{n+1},\ldots,b_{n+1}}_{Q}, \underbrace{a_{Q+n+1},\ldots,a_N}_{N-Q-n}]$.

2) For $n \in \aleph^{N-2}_{N-Q}$, we have $a_N \leq b_{n+1}$. Due to $a_i \leq a_N$ for $i \in \aleph^{N-1}_1$, we have $a_i \leq b_{n+1}$ for all $i \in \aleph^{N-1}_1$. Since any $(\xi_{n+1},\ldots,\xi_N) \in \Pi^{(N-n)}_{\boldsymbol{\psi}^N_{n,a_N}}$ belongs to a Cartesian product of $(N-n)$ intervals (a hyper-rectangle) $[b_{n+1},\xi_{n+2}] \times \ldots \times [b_{n+1},\xi_N] \times [b_{n+1},b_N]$ having the same lower limit b_{n+1}, this case is the same as Case 1. Equivalently, $\Xi^{(N)}_n = \Omega^{(n)} \times \Pi^{(N-n)}_{\boldsymbol{\psi}^N_{n,a_N}}$ with $\boldsymbol{\psi}^N_{n,a_N} = b_{n+1}\mathbf{1}_{N-n}$. Summarizing the preceding results for Case 2, we have

$$\int_{\Xi^{(N)}_n} \cdots \int d\boldsymbol{\xi}_N = \int_{\Pi^{(N-n)}_{\boldsymbol{\psi}^N_{n,a_N}}} \cdots \int d\xi_{n+1}\cdots d\xi_N \times \int_{\Omega^{(n)}} \cdots \int d\xi_1 \cdots d\xi_n = f^{(N-n)}_{\boldsymbol{\psi}^N_{n,a_N}}(b_N) I^{(n)} \quad (46)$$

where $\boldsymbol{\psi}^N_{n,a_N} = [\underbrace{b_{n+1},\ldots,b_{n+1}}_{Q}, \underbrace{a_{Q+n+1},\ldots,a_N}_{N-Q-n}]$ for $n \in \aleph^{N-Q-1}_0$ and $\boldsymbol{\psi}^N_{n,a_N} = b_{n+1}\mathbf{1}_{N-n}$ for $n \in \aleph^{N-2}_{N-Q}$.

The proof follows immediately from (43), (45), and (46) and the fact that the first term on the RHS of (43) is $f^{(N)}_{\boldsymbol{a}_0^N}(b_N)$. ■

Appendix C
Proof of Lemma 3

Though the idea of the proof can be extended to a general case of $a_{N-1} \leq c$ and $a_N \leq d$, we will consider the following two cases: Case 1: $c := \bar{\gamma}_N \leq b_N$ and $d := \infty$, and Case 2: $c := a_N$ and $d := b_N$, which correspond to (21) and (22) respectively. Define the following sets $\Theta^{(N)}_{c,d} := \{(\xi_1,\ldots,\xi_N) : \xi_0 \leq \xi_1 \leq \ldots \leq \xi_N; a_i < \xi_i \leq \xi_{i+1}, i \in \aleph^{N-1}_1, c < \xi_N < d\}$, and $\Phi^{(N,n)}_{c,d} := \{(\xi_1,\ldots,\xi_N) : (\xi_1,\ldots,\xi_N) \in \Theta^{(N)}_{c,d}; a_i < \xi_i < b_i, i \in \aleph^n_1; b_{n+1} < \xi_{n+1} \leq \xi_{n+2}\}$, where $\Phi^{(N,n)}_{c,d}$ are non-overlapping subsets of $\Theta^{(N)}_{c,d}$ for $n \in \aleph^{N-2}_0$. The integral over $\Theta^{(N)}_{c,d}$ can be readily computed as

$$\int_{\Theta^{(N)}_{c,d}} \cdots \int e^{-\theta\xi_N} d\boldsymbol{\xi}_N = \int_c^d e^{-\theta\xi_N} f^{(N-1)}_{\boldsymbol{a}_0^{N-1}}(\xi_N) d\xi_N = \sum_{i=1}^{N} \theta^{-i} \left[f^{(N-i)}_{\boldsymbol{a}_0^{N-i}}(c) e^{-\theta c} - f^{(N-i)}_{\boldsymbol{a}_0^{N-i}}(d) e^{-\theta d} \right] \quad (47)$$

where (47) is obtained by using integration by parts repeatedly and the differential property $df^{(k)}_{\boldsymbol{\chi}_k}(\xi)/d\xi = f^{(k-1)}_{\boldsymbol{\chi}_{k-1}}(\xi)$.

- Case 1: $a_N \leq \bar{\gamma}_N \leq b_N$ and $d = \infty$. Similarly to the argument used in Lemma 2, we have $\Upsilon^{(N)}_{\bar{\gamma}_N,\infty} = \Theta^{(N)}_{\bar{\gamma}_N,\infty} \bigcap \big(\cup_{n=0}^{N-2} \Phi^{(N,n)}_{\bar{\gamma}_N,\infty}\big)^c$ and thus we have

$$J^{(N)}_{\bar{\gamma}_N,\infty}(\theta) = \int_{\Theta^{(N)}_{\bar{\gamma}_N,\infty}} \cdots \int e^{-\theta\xi_N} d\boldsymbol{\xi}_N - \sum_{n=0}^{N-2} \int_{\Phi^{(N,n)}_{\bar{\gamma}_N,\infty}} \cdots \int e^{-\theta\xi_N} d\boldsymbol{\xi}_N.$$

Substituting $c = \bar{\gamma}_N$ and $d = \infty$ in (47) and using the fact that $e^{-\theta d}$ is zero for $\theta > 0$, we have

$$\int_{\Theta^{(N)}_{\bar{\gamma}_N,\infty}} \cdots \int e^{-\theta\xi_N} d\boldsymbol{\xi}_N = \sum_{i=1}^{N} \theta^{-i} f^{(N-i)}_{\boldsymbol{a}_0^{N-i}}(\bar{\gamma}_N) e^{-\theta\bar{\gamma}_N}.$$

1) For $\bar{\gamma}_N \leq b_1$, we have $b_1 \geq a_N$ since $\bar{\gamma}_N \geq a_N$. Since $\xi_n \leq b_n < b_{n+1}$, we have $\Phi^{(N,n)}_{\bar{\gamma}_N,\infty} = \Omega^{(n)} \times \Pi^{(N-n)}_{b_{n+1}\mathbf{1}_{N-n}}$ and the integrations over $\Omega^{(n)}$ and $\Pi^{(N-n)}_{b_{n+1}\mathbf{1}_{N-n}}$ are separable. Thus, applying integration by parts and the fact $f^{(k)}_{\boldsymbol{\chi}_k}(\chi_k) = 0$, we obtain

$$\begin{aligned}
&\int_{\Phi^{(N,n)}_{\bar{\gamma}_N,\infty}} \cdots \int e^{-\theta\xi_N} d\boldsymbol{\xi}_N \\
&= \int_{\Pi^{(N-n)}_{b_{n+1}\mathbf{1}_{N-n}}} \cdots \int e^{-\theta\xi_N} d\xi_{n+1} \cdots d\xi_N \times \int_{\Omega^{(n)}} \cdots \int d\xi_1 \cdots d\xi_n \\
&= I^{(n)} \int_{b_{n+1}}^{\infty} e^{-\theta\xi_N} f^{(N-n-1)}_{b_{n+1}\mathbf{1}_{N-n-1}}(\xi_N) d\xi_N \\
&= I^{(n)} \theta^{n-N} e^{-\theta b_{n+1}}. \qquad (48)
\end{aligned}$$

2) For $\bar{\gamma}_N > b_1$, we have $s \geq 1$ since $b_s < \bar{\gamma}_N \leq b_{s+1}$. Similarly to the argument used in Case 2 of the proof of Lemma 2, we have $\Phi^{(N)}_n = \Omega^{(n)} \times \Pi^{(N-n)}_{\boldsymbol{\psi}^N_{n,\bar{\gamma}_N}}$,

$$\int_{\Phi^{(N,n)}_{\bar{\gamma}_N,\infty}} \cdots \int e^{-\theta\xi_N} d\boldsymbol{\xi}_N = I^{(n)} \times \sum_{i=1}^{N-n} \begin{cases} \theta^{-i} f^{(N-n-i)}_{\boldsymbol{\psi}^{N-i}_{n,\bar{\gamma}_N}}(\bar{\gamma}_N) e^{-\theta\bar{\gamma}_N}, n \in \aleph_0^{s-1} \\ \theta^{-i} f^{(N-n-i)}_{\boldsymbol{\psi}^{N-i}_{n,\bar{\gamma}_N}}(b_{n+1}) e^{-\theta b_{n+1}}, n \in \aleph_s^{N-2}. \end{cases} \qquad (49)$$

This concludes the proof for Case 1.

- Case 2: $c = a_N$ and $b = b_N$. Similarly to the method used in Case 1, we have $\Upsilon^{(N)}_{a_N,b_N} = \Theta^{(N)}_{a_N,b_N} \bigcap \big(\cup_{n=0}^{N-2} \Phi^{(N,n)}_{a_N,b_N}\big)^c$ and thus we can express $J^{(N)}_{a_N,b_N}(\theta)$ as

$$J^{(N)}_{a_N,b_N}(\theta) = \int_{\Theta^{(N)}_{a_N,b_N}} \cdots \int e^{-\theta\xi_N} d\boldsymbol{\xi}_N - \mathbb{I}_{\{N\geq 2\}} \sum_{n=0}^{N-2} \int_{\Phi^{(N,n)}_{a_N,b_N}} \cdots \int e^{-\theta\xi_N} d\boldsymbol{\xi}_N. \qquad (50)$$

The rest of the proof is analogous to that in Case 1. The key difference is that in Case 2, the term $e^{-\theta d}$ is no longer zero. From (47), the first term on the RHS of (50) can be readily obtained as

$$\int_{\Theta^{(N)}_{a_N,b_N}} \cdots \int e^{\theta\xi_N} d\boldsymbol{\xi}_N = \sum_{i=1}^{N} \theta^{-i} \big[f^{(N-i)}_{\boldsymbol{a}_0^{N-i}}(a_N) e^{\theta a_N} - f^{(N-i)}_{\boldsymbol{a}_0^{N-i}}(b_N) e^{-\theta b_N} \big]. \qquad (51)$$

Since $b_{N-Q} < a_N \leq b_{N-Q+1}$, we have $s = N - Q$ in this case. Similarly to the method used to derive (48) and (49), we have

$$\int_{\Phi^{(N,n)}_{a_N,b_N}} \cdots \int e^{-\theta\xi_N} d\boldsymbol{\xi}_N = \begin{cases} I^{(n)} \Big[\theta^{n-N} e^{-\theta b_{n+1}} - \sum_{i=1}^{N-n} \theta^{-i} \\ f^{(N-n-i)}_{b_{n+1}\mathbf{1}_{N-n-i}}(b_N) e^{-\theta d} \Big], a_N \leq b_1, n \in \aleph_0^{N-2}; \\ I^{(n)} \sum_{i=1}^{N-n} \theta^{-i} \Big[f^{(N-n-i)}_{\boldsymbol{\psi}^{N-i}_{n,a_N}}(a_N) e^{-\theta a_N} - \\ f^{(N-n-i)}_{\boldsymbol{\psi}^{N-i}_{n,a_N}}(b_N) e^{-\theta b_N} \Big], a_N > b_1, n \in \aleph_0^{N-Q-1}; \\ I^{(n)} \Big[\theta^{n-N} e^{-\theta b_{n+1}} - \sum_{i=1}^{N-n} \theta^{-i} \\ f^{(N-n-i)}_{b_{n+1}\mathbf{1}_{N-n-i}}(b_N) e^{-\theta b_N} \Big], a_N > b_1, n \in \aleph_{N-Q}^{N-2}. \end{cases} \qquad (52)$$

The proof for Case 2 follows clearly from (50)-(52). ■

APPENDIX D
PROOF OF PROPERTY 2

Note that $F_N = \mathcal{A}_N^{l_N} \cap \mathcal{B}_N^{l_N}$ and $\tilde{F}_N = \tilde{\mathcal{A}}_N^{l_N} \cap \tilde{\mathcal{B}}_N^{l_N}$. Applying the inclusion-exclusion identity [24, p. 80], we have $P_{H_1}(F_N) = P_{H_1}(\mathcal{A}_N^{l_N}) + P_{H_1}(\mathcal{B}_N^{l_N}) - P_{H_1}(\mathcal{A}_N^{l_N} \cup \mathcal{B}_N^{l_N})$ and $P_{H_1}(\tilde{F}_N) = P_{H_1}(\tilde{\mathcal{A}}_N^{l_N}) + P_{H_1}(\tilde{\mathcal{B}}_N^{l_N}) - P_{H_1}(\tilde{\mathcal{A}}_N^{l_N} \cup \tilde{\mathcal{B}}_N^{l_N})$. Thus, by using the triangle inequality, we have

$$\begin{aligned}
&|P_{H_1}(F_N) - P_{H_1}(\tilde{F}_N)| \leq \\
&|P_{H_1}(\mathcal{A}_N^{l_N}) - P_{H_1}(\tilde{\mathcal{A}}_N^{L_N})| + |P_{H_1}(\mathcal{B}_N^{L_N}) - P_{H_1}(\tilde{\mathcal{B}}_N^{L_N})| \\
&+ |P_{H_1}(\mathcal{A}_N^{L_N} \cup \mathcal{B}_N^{L_N}) - P_{H_1}(\tilde{\mathcal{A}}_N^{L_N} \cup \tilde{\mathcal{B}}_N^{L_N})|. \qquad (53)
\end{aligned}$$

Since $1 - \epsilon/(3M) \leq P_{H_1}(\mathcal{A}_N^{L_N}) \leq 1$ and $1 - \epsilon/(3M) \leq P_{H_1}(\tilde{\mathcal{A}}_N^{L_N}) \leq 1$, we have $1 - \epsilon/(3M) \leq P_{H_1}(\mathcal{A}_N^{L_N}) \leq P_{H_1}(\mathcal{A}_N^{L_N} \cup \mathcal{B}_N^{L_N}) \leq 1$ and $1 - \epsilon/(3M) \leq P_{H_1}(\tilde{\mathcal{A}}_N^{L_N}) \leq P_{H_1}(\tilde{\mathcal{A}}_N^{L_N} \cup \tilde{\mathcal{B}}_N^{L_N}) \leq 1$. It can be readily inferred from the above inequalities that $|P_{H_1}(\mathcal{A}_N^{L_N}) - P_{H_1}(\tilde{\mathcal{A}}_N^{L_N})| \leq \epsilon/(3M)$ and $|P_{H_1}(\mathcal{A}_N^{L_N} \cup \mathcal{B}_N^{L_N}) - P_{H_1}(\tilde{\mathcal{A}}_N^{L_N} \cup \tilde{\mathcal{B}}_N^{L_N})| \leq \epsilon/(3M)$. This, along with the inequality (53) and the assumption $|P_{H_1}(\mathcal{B}_N^{L_N}) - P_{H_1}(\tilde{\mathcal{B}}_N^{L_N})| \leq \epsilon/(3M)$, implies that $|P_{H_1}(F_N) - P_{H_1}(\tilde{F}_N)| < \epsilon/M$. Hence, we have $|\beta_{\text{ssct}} - \tilde{\beta}_{\text{ssct}}| \leq \sum_{i=1}^{M} |P_{H_1}(F_N) - P_{H_1}(\tilde{F}_N)| \leq \epsilon$. ■

REFERENCES

[1] Y.-C. Liang, Y. Zeng, E. Peh, and A. Hoang, "Sensing-throughput tradeoff for cognitive radio networks," *IEEE Trans. Wireless Commun.*, vol. 7, no. 4, pp. 1326–1337, Apr. 2008.

[2] Z. Quan, S. Cui, and A. Sayed, "Optimal linear cooperation for spectrum sensing in cognitive radio networks," *IEEE J. Sel. Topics Signal Process.*, vol. 2, no. 1, pp. 28–40, Feb. 2008.
[3] S. J. Kim and G. B. Giannakis, "Rate-optimal and reduced-complexity sequential sensing algorithms for cognitive OFDM radios," in *Proc. 43rd Conf. Info. Sci. Syst.*, Mar. 2009.
[4] H. S. Chen, W. Gao, and D. G. Daut, "Signature based spectrum sensing algorithms for IEEE 802.22 WRAN," in *Proc. IEEE Int. Conf. Commun. (ICC)*, June 2008, pp. 6487–6492.
[5] H. Urkowitz, "Energy detection of unknown deterministic signals," *Proc. IEEE*, vol. 55, no. 4, pp. 523–531, Apr. 1967.
[6] J. Lundén, V. Koivunen, A. Huttunen, and H. V. Poor, "Spectrum sensing in cognitive radios based on multiple cyclic frequencies," in *Proc. IEEE Cognitive Radio Oriented Wireless Netw. Commun. (CrownCom)*, Aug. 2007, pp. 37–43.
[7] H. Li, H. Dai, and C. Li, "Collaborative quickest spectrum sensing via random broadcast in cognitive radio systems," *IEEE Trans. Wireless Commun.*, vol. 9, no. 7, pp. 2338–2348, July 2010.
[8] G. Noh, H. Wang, J. Jo, B.-H. Kim, and D. Hong, "Reporting order control for fast primary detection in cooperative spectrum sensing," *IEEE Trans. Veh. Technol.*, vol. 60, no. 8, pp. 4058–4063, Oct. 2011.
[9] B. Wang and K. J. R. Liu, "Advances in cognitive radio networks: A survey," *IEEE J. Sel. Topics Signal Process.*, vol. 5, no. 1, pp. 5–23, Feb. 2011.
[10] L. Lu, X. Zhou, U. Onunkwo, and G. Y. Li, "Ten years of research in spectrum sensing and sharing in cognitive radio," *EURASIP J. Wireless Commun. Netw.*, Jan. 2012.
[11] T. H. Lim, R. Zhang, Y.-C. Liang, and H. Zeng, "GLRT-based spectrum sensing for cognitive radio," in *Proc. IEEE Global Telecommun. Conf. (GLOBECOM)*, Nov. 2008, pp. 1–5.
[12] J. Kim and J. G. Andrews, "Sensitive white space detection with spectral covariance sensing," *IEEE Trans. Wireless Commun.*, vol. 9, no. 9, pp. 2945–2955, Sep. 2010.
[13] J. Kim, C.-B. Chae, and J. G. Andrews, "Cooperative spectral covariance sensing under correlated shadowing," *IEEE Trans. Wireless Commun.*, vol. 10, no. 11, pp. 3589–3593, Nov. 2011.
[14] Y. Zeng and Y. Liang, "Covariance based signal detections for cognitive radio," in *Proc. IEEE Int. Symp. New Frontiers Dynamic Spectrum Access Netw. (DySPAN)*, 2007, pp. 202–207.
[15] R. Tandra and A. Sahai, "SNR walls for signal detection," *IEEE J. Sel. Topics Signal Process.*, vol. 2, no. 1, pp. 4–17, Feb. 2008.
[16] N. Kundargi and A. Tewfik, "Hierarchical sequential detection in the context of dynamic spectrum access for cognitive radios," in *Proc. IEEE 14th Int. Conf. Electronics, Circuits Syst.*, Dec. 2007, pp. 514–517.
[17] B. Chen, J. Park, and K. Bian, "Robust distributed spectrum sensing in cognitive radio networks," Dept. of Electrical and Computer Engineering, Virginia Tech, Tech. Rep. TR-ECE-06-07, July 2006.
[18] A. Wald, "Sequential tests of statistical hypothesis," *Annals Math. Stat.*, vol. 17, pp. 117–186, 1945.
[19] A. Wald and J. Wolfowitz, "Optimum character of the sequential probability ratio test," *Annals Math. Stat.*, vol. 19, pp. 326–329, 1948.
[20] R. C. Woodall and B. M. Kurkjian, "Exact operating characteristic for truncated sequential life tests," *Annals Math. Stat.*, vol. 33, pp. 1403–1412, 1962.
[21] L. A. Aroian, "Sequential analysis, direct method," *Technometrics*, vol. 10, no. 1, pp. 125–132, Feb. 1968.
[22] N. L. Johnson, "Sequential analysis: A survey," *J. Royal Statistical Society. Series A (General)*, no. 3, pp. 372–411, 1961.
[23] S. M. Pollock and D. Golhar, "Efficient recursions for truncation of the SPRT," Dept. of Industrial and Operations Engineering, University of Michigan, Tech. Rep. No. 85-24, Aug. 1985.
[24] B. Fristedt and L. Gray, *A Modern Approach to Probability Theory*. Boston: Birkhäuser, 1997.

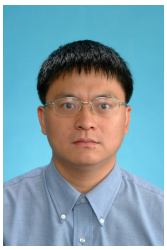

Yan Xin (SM'10) received the Ph.D. degree in electrical engineering from the University of Minnesota, Minneapolis, MN, in 2003. From 2004 to 2008, he was an assistant professor in the Department of Electrical and Computer Engineering, National University of Singapore. He was a research staff member at NEC Laboratories America Inc., Princeton, New Jersey, from 2008 to 2012. He is now with Samsung Research America Dallas (SRA-D), Richardson, Texas. His research interests include MIMO communications, cognitive radio, and network information theory. He received the 2004 IEEE Marconi Prize Paper Award in wireless communications from the IEEE Communications Society.

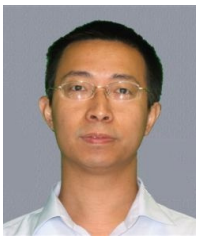

Honghai Zhang received the B.S. degree from the University of Science and Technology of China and the Ph.D. degree from the Department of Computer Science at the University of Illinois at Urbana-Champaign. He was a recipient of the Vodafone Fellowship during his Ph.D. study. He is currently a software engineer at Google. Previously, he was a Research Staff Member with NEC Laboratories America. Prior to that, he was in the Wireless Advanced Technology Laboratory of Alcatel-Lucent. His research interests include mobile web and mobile wireless networks.

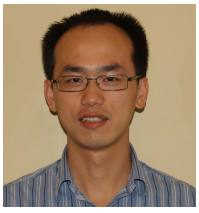

Lifeng Lai (M'07) received the B.E. and M. E. degrees from Zhejiang University, Hangzhou, China, in 2001 and 2004 respectively, and the Ph.D. degree from The Ohio State University at Columbus, OH, in 2007. He was a postdoctoral research associate at Princeton University from 2007 to 2009, and was an assistant professor at the University of Arkansas, Little Rock, from 2009 to 2012. Since Aug. 2012, he has been an assistant professor at Worcester Polytechnic Institute. Dr. Lai's research interests include information theory, stochastic signal processing and its applications in wireless communications, security, and other related areas.

Dr. Lai was a Distinguished University Fellow of the Ohio State University from 2004 to 2007. He is a co-recipient of the Best Paper Award from the IEEE Global Communications Conference (Globecom) in 2008, the Best Paper Award from the IEEE International Conference on Communications (ICC) in 2011, and the Best Paper Award from IEEE Smart Grid Communications (SmartGridComm) in 2012. He received the National Science Foundation CAREER Award in 2011 and the Northrop Young Researcher Award in 2012. He served as a Guest Editor for the IEEE JOURNAL ON SELECTED AREAS IN COMMUNICATIONS, SPECIAL ISSUE ON SIGNAL PROCESSING TECHNIQUES FOR WIRELESS PHYSICAL LAYER SECURITY. He is currently serving as an Editor for the IEEE TRANSACTIONS ON WIRELESS COMMUNICATIONS.